A Run-Group Proposal Submitted to PAC 44

Measurement of Deep Exclusive π^- Production using a Transversely Polarized ^{3}He Target and the SoLID Spectrometer

May 4, 2017

J. Arrington, K. Hafidi, P. Reimer, Z. Ye*
Argonne National Laboratory, Physics Division, Argonne, IL, USA

Z. Ahmed*, G.R. Ambrose, S. Basnet, R.S. Evans, G.M. Huber†, W. Li, D. Paudyal, Z. Papandreou
University of Regina, Regina, SK, Canada

H. Gao, X. Li, T. Liu, C. Peng, W. Xiong, X.F. Yan, Z. Zhao
Duke University, Durham, NC, USA

A. Camsonne, J-P. Chen, S. Covrig-Dusa, D. Gaskell
Jefferson Lab, Newport News, VA, USA

T. Brecelj, M. Mihovilovič, S. Širca, S. Štajner
Jožef Stefan Institute and University of Ljubljana, Slovenia

K. Aniol
California State University – Los Angeles, Los Angeles, CA, USA

M. Boer
Los Alamos National Laboratory, Physics Division, Los Alamos, NM, USA

D. Dutta, L. Ye
Mississippi State University, Mississippi State, MS, USA

C. E. Hyde, F.R. Wesselmann
Old Dominion University, Norfolk, VA, USA

P. Markowitz
Florida International University, Miami, FL, USA

V. Sulkosky
University of Virginia, Charlottesville, VA, USA

E. Voutier
Institut de Physique Nucléaire IN2P3/CNRS, Université Paris Sud, Orsay, France

† Contact person , * Spokesperson

Contents

Abstract

We propose to measure the transverse nucleon, single-spin asymmetry $A_{UT}^{sin(\phi-\phi_s)}$ in the exclusive $\vec{n}(e,e'\pi^-)p$ reaction, during the transversely polarized ^{3}He target SIDIS experiment (i.e. E12-10-006 [1]) with SoLID [2]. This polarization observable has been noted as being sensitive to the spin-flip generalized parton distribution (GPD) $\tilde{E}$, and factorization studies have indicated that precocious scaling is likely to set in at moderate $Q^2 \sim 2-4$ GeV^2, as opposed to the absolute cross section, where scaling is not expected until $Q^2 > 10$ GeV^2. Furthermore, this observable has been noted as being important for the reliable extraction of the charged pion form factor from pion electroproduction. The asymmetry data are projected to be of much higher quality than a pioneering measurement by HERMES [3].

This measurement is complementary to a proposal reviewed by PAC39 [4] for the SHMS+HMS in Hall C. The asymmetry that is most sensitive to $\tilde{E}$ is the longitudinal photon, transverse nucleon, single-spin asymmetry $A_L^{\perp}$ in exclusive charged pion electroproduction. The SHMS+HMS allow the L–T separation needed to reliably measure this quantity. However, the limited detector acceptance and the error-magnification inherent in an L–T separation necessitates the use of a next generation, externally polarized, continuous flow, high luminosity $^3\tilde{\text{H}}$e target based on a large volume polarizer and compressor being developed at the University of New Hampshire.

A wide $-t$ coverage is needed to obtain a good understanding of the asymmetry. Thus, it has always been intended to complement the SHMS+HMS $A_L^{\perp}$ measurement with an unseparated $A_{UT}^{sin(\phi-\phi_s)}$ measurement using a large solid angle detector. The high luminosity capabilities of SoLID make it well-suited for this measurement. Since an L–T separation is not possible with SoLID, the observed asymmetry is expected to be diluted by the ratio of the longitudinal cross section to the unseparated cross section. This was also true for the pioneering HERMES measurements, which provided a valuable constraint to models for the $\tilde{E}$ GPD. Simultaneously, the $A_{UT}^{sin(\phi_s)}$ asymmetry will be measured, which provides valuable information on transverse photon contributions at small $-t$.

In order to assure a clean measurement of exclusive π^- production, it is required to detect the recoil proton from the $\vec{n}(e,e'\pi^-)p$ reaction. We propose to analyze the E12-10-006 event files off-line to look for $e-\pi^--p$ triple coincidence events in SoLID for the case where the proton is emitted $8^o < \theta < 24^o$. This has no impact upon E12-01-006 whatsoever, and yields valuable unseparated asymmetry data.

1 Scientific Justification

1.1 Generalized Parton Distributions and Contribution from the Pion Pole

In recent years, much progress has been made in the theory of generalized parton distributions (GPDs). Unifying the concepts of parton distributions and of hadronic form factors, they contain a wealth of information about how quarks and gluons make up hadrons. The key difference between the usual parton distributions and their generalized counterparts can be seen by representing them in terms of the quark and gluon wavefunctions of the hadron. While the usual parton distributions are obtained from the squared hadron wavefunction representing the probability to find a parton with specified polarization and longitudinal momentum fraction x in the fast moving hadron (Fig. 1a), GPDs represent the interference of different wavefunctions, one where the parton has momentum fraction $x+\xi$ and one where this fraction is $x-\xi$ (Fig. 1b). GPDs thus correlate different parton configurations in the hadron at the quantum mechanical level. A special kinematic regime is probed in deep exclusive meson production, where the initial hadron emits a quark-antiquark or gluon pair (Fig. 1c). This has no counterpart in the usual parton distributions and carries information about $q\bar{q}$ and gg-components in the hadron wavefunction.

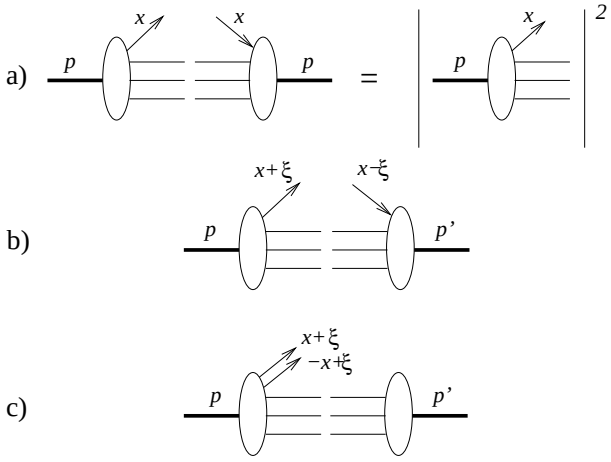

Figure 1: (a) Usual parton distribution, representing the probability to find a parton with momentum fraction x in the nucleon. (b) GPD in the region where it represents the emission of a parton with momentum fraction $x+\xi$ and its reabsorption with momentum fraction $x-\xi$. (c) GPD in the region where it represents the emission of a quark-antiquark pair, and has no counterpart in the usual parton distributions. This figure has been adapted from Ref. [5].

Apart from the momentum fraction variables x and ξ, GPDs depend on the four momentum transfer t. This is an independent variable, because the momenta p and p' may differ in either their longitudinal or transverse components. GPDs thus interrelate the longitudinal and transverse momentum structure of partons within a fast moving hadron.

In order to access the physics contained within GPDs, one is restricted to the hard scattering regime. An important feature of hard scattering reactions is the possibility to separate clearly the perturbative and non-perturbative stages of the interaction. Qualitatively speaking, the presence of a hard probe allows one to create small size quark-antiquark and gluon configurations, whose interactions are described by perturbative QCD (pQCD). The non-perturbative stage of the reaction describes how the hadron reacts to this configuration, or how this probe is transformed into hadrons. This separation is the so-called factorization property

of hard reactions. Deep Exclusive Meson electro-Production (DEMP) was first shown to be factorizable in Ref. [6]. This factorization applies when the virtual photon is longitudinally polarized, which is more probable to produce a small size configuration compared to a transversely polarized photon.

GPDs are universal quantities and reflect the structure of the nucleon independently of the reaction which probes the nucleon. At leading twist-2 level, the nucleon structure information can be parameterized in terms of four quark chirality conserving GPDs, denoted H, E, $\tilde{H}$ and $\tilde{E}$. H and E are summed over quark helicity, while $\tilde{H}$ and $\tilde{E}$ involve the difference between left and right handed quarks. H and $\tilde{H}$ conserve the helicity of the proton, while E and $\tilde{E}$ allow for the possibility that the proton helicity is flipped. Because quark helicity is conserved in the hard scattering regime, the produced meson acts as a helicity filter. In particular, leading order QCD predicts that vector meson production is sensitive only to the unpolarized GPDs, H and E, whereas pseudoscalar meson production is sensitive only to the polarized GPDs, $\tilde{H}$ and $\tilde{E}$. In contrast, deeply virtual Compton scattering (DVCS) depends at the same time on both the polarized ($\tilde{H}$ and $\tilde{E}$) and the unpolarized (H and E) GPDs. This makes DEMP reactions complementary to the DVCS process, as it provides an additional tool to disentangle the different GPDs [7].

Besides coinciding with the parton distributions at vanishing momentum transfer ξ, the GPDs have interesting links with other nucleon structure quantities. Their first moments are related to the elastic form factors of the nucleon through model-independent sum rules [8]:

$$\sum_q e_q \int_{-1}^{+1} dx H^q(x,\xi,t) = F_1(t), \tag{1}$$

$$\sum_q e_q \int_{-1}^{+1} dx E^q(x,\xi,t) = F_2(t), \tag{2}$$

$$\sum_q e_q \int_{-1}^{+1} dx \tilde{H}^q(x,\xi,t) = G_A(t), \tag{3}$$

$$\sum_q e_q \int_{-1}^{+1} dx \tilde{E}^q(x,\xi,t) = G_P(t), \tag{4}$$

where e_q is the charge of the relevant quark, $F_1(t)$, $F_2(t)$ are the Dirac and Pauli elastic nucleon form factors, and $G_A(t)$, $G_P(t)$ are the isovector axial and pseudoscalar nucleon form factors. The t-dependence of $G_A(t)$ is poorly known, and although $G_P(t)$ is an important quantity, it remains highly uncertain because it is negligible at the momentum transfer of β-decay [9]. Because of partial conservation of the axial current (PCAC), $G_P(t)$ alone receives contributions from $J^{PG} = 0^{--}$ states [10], which are the quantum numbers of the pion, and so $\tilde{E}$ contains an important pion pole contribution (Fig. 2a).

Accordingly, Refs. [11, 12] have adopted the pion pole-dominated ansatz

$$\tilde{E}^{ud}(x,\xi,t) = F_\pi(t) \frac{\theta(\xi > |x|)}{2\xi} \phi_\pi(\frac{x+\xi}{2\xi}), \tag{5}$$

where $F_\pi(t)$ is the pion electromagnetic form factor, and ϕ_π is the pion distribution amplitude. For the kinematic region accessible until the construction of the EIC, the best estimate of $\tilde{E}$ is obtained if one replaces the perturbative (or one-gluon exchange) expression for F_π with a parameterization based on the experimental form factor [13]. Regardless of which expression is used, $\tilde{E}$ cannot be related to already known parton distributions, and so experimental information about $\tilde{E}$ via DEMP can provide new information on nucleon structure which is unlikely to be available from any other source.

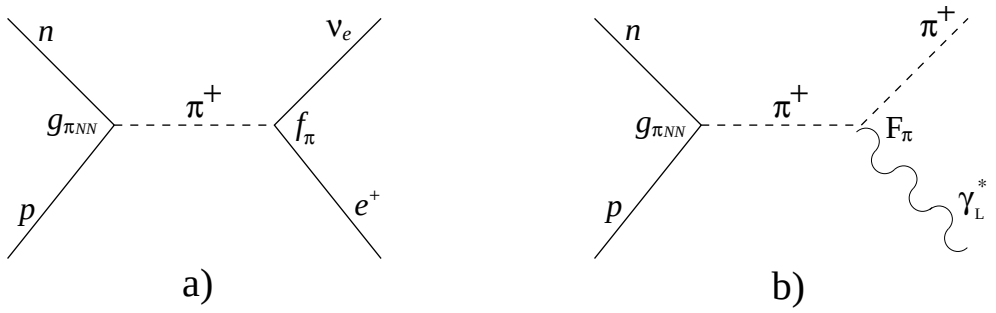

Figure 2: (a) Pion pole contribution to $G_P(t)$, and hence to $\tilde{E}$. (b) Pion pole contribution to meson electroproduction at low $-t$.

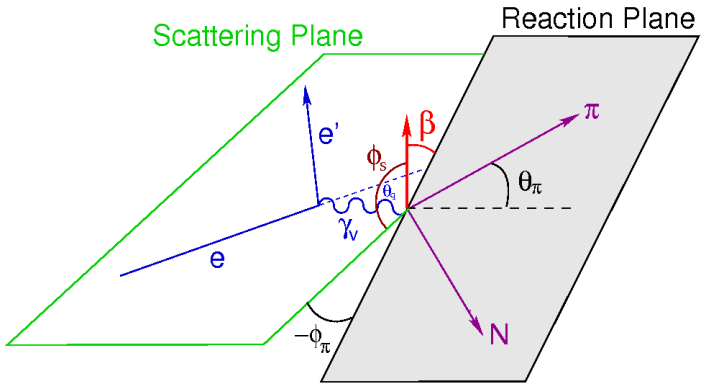

Figure 3: Scattering and hadronic reaction planes for exclusive $\vec{N}(e,e'\pi)N'$. $\beta = (\phi - \phi_s)$ is the angle between the target nucleon polarization vector and the reaction plane. θ_q is the scattering angle of the virtual photon.

1.2 Single spin asymmetry in exclusive pion electroproduction

Frankfurt et al. [14] have considered a specific polarization observable which is the most sensitive observable to probe the spin-flip $\tilde{E}$. This variable is the single-spin asymmetry for exclusive charged pion production, $\vec{p}(e,e'\pi^+)n$ or $\vec{n}(e,e'\pi^-)p$, from a transversely polarized nucleon target, and is defined [12] as

$$A_L^\perp = \left(\int_0^\pi d\beta \frac{d\sigma_L^\pi}{d\beta} - \int_\pi^{2\pi} d\beta \frac{d\sigma_L^\pi}{d\beta}\right)\left(\int_0^{2\pi} d\beta \frac{d\sigma_L^\pi}{d\beta}\right)^{-1}, \tag{6}$$

where $d\sigma_L^\pi$ is the exclusive charged pion electroproduction cross section using longitudinally polarized photons and β is the angle between the nucleon polarization vector and the reaction plane (Fig. 3).

This asymmetry is related to the parton-helicity-conserving part of the scattering process and is sensitive to the interference between $\tilde{H}$ and $\tilde{E}$ [14, 15]:

$$A_L^\perp = \frac{\sqrt{-t'}}{m_p} \frac{\xi\sqrt{1-\xi^2}\ \mathrm{Im}(\tilde{E}^*\tilde{H})}{(1-\xi^2)\tilde{H}^2 - \frac{t\xi^2}{4m_p}\tilde{E}^2 - 2\xi^2 \mathrm{Re}(\tilde{E}^*\tilde{H})}. \tag{7}$$

Frankfurt et al. [14] have shown that this asymmetry must vanish if $\tilde{E}$ is zero. If $\tilde{E}$ is not zero, the asymmetry will display a sinβ dependence. Their predicted asymmetry using the $\tilde{E}$ ansatz from Ref. [17] is shown in Fig. 4. This calculation is Q^2-independent, depending only on how well the soft contributions cancel in the asymmetry.

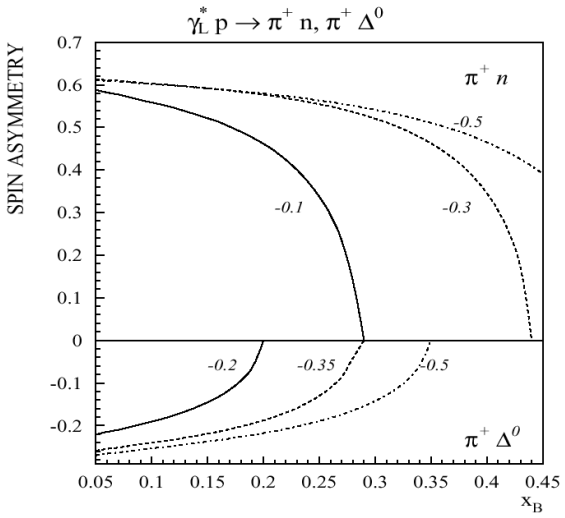

Figure 4: Transverse single-spin asymmetry for the longitudinal electroproduction of $\pi^+ n$ and $\pi^+\Delta^0$ at different values of t [indicated on the curves in GeV^2]. The asymmetry drops to zero at the parallel kinematic limit, which is different for each t value, because the definition of β is ill-defined at this point. This figure is taken from Ref. [18].

It seems likely that a precocious factorization of the meson production amplitude into three parts – the overlap integral between the photon and pion wave functions, the hard interaction, and the GPD – will lead to a precocious scaling of $A_L^\perp$ as a function of Q^2 at moderate $Q^2 \sim 2-4$ GeV^2 [14]. This precocious scaling arises from the fact that higher twist corrections, which are expected to be significant at low Q^2, will likely cancel when one examines the ratio of two longitudinal observables. In contrast, the onset of scaling for the absolute cross section is only expected for much larger values of $Q^2 > 10$ GeV^2.

This point is made clear in Fig. 5. This figure shows renormalon model calculations [19] of both the asymmetry and the longitudinal cross section at $Q^2 = 4$ GeV^2. While the magnitude of the cross section changes significantly when taking into account the twist-four corrections, $A_L^\perp$ is essentially insensitive to them and displays the expected precocious scaling. The relatively low value of Q^2 for the expected onset of precocious scaling is important, because it will be experimentally accessible after the Jefferson Lab 12 GeV upgrade. This places $A_L^\perp$ among the most important GPD measurements that can be made in the meson scalar. If precocious scaling cannot be experimentally demonstrated in this ratio of two cross sections, then it may not be possible to determine GPDs from DEMP data.

Refs. [7] and [18] also point out that the study of the transverse target single-spin asymmetry versus t is important for the reliable extraction of the pion form factor from electroproduction experiments (Fig. 2b). Investigations of hard exclusive π^+ electroproduction using a pQCD factorization model [20, 21] find that at $x_B = 0.3$ and $-t = -t_{min}$, the pion pole contributes about 80% of the longitudinal cross section. Since the longitudinal photon transverse single-spin asymmetry is an interference between pseudoscalar and pseudovector contributions, its measurement would help constrain the non-pole pseudovector contribution, and so assist the more reliable extraction of the pion form factor. The upper $Q^2 = 6$ GeV^2 limit of the approved pion form factor measurements in the JLab 12 GeV program [22] is dictated primarily by the requirement $-t_{min} < 0.2$ GeV^2, to keep non-pion pole contributions to σ_L at an acceptable level [21]. Transverse target single-spin asymmetry studies versus t may eventually allow, with theoretical input, the

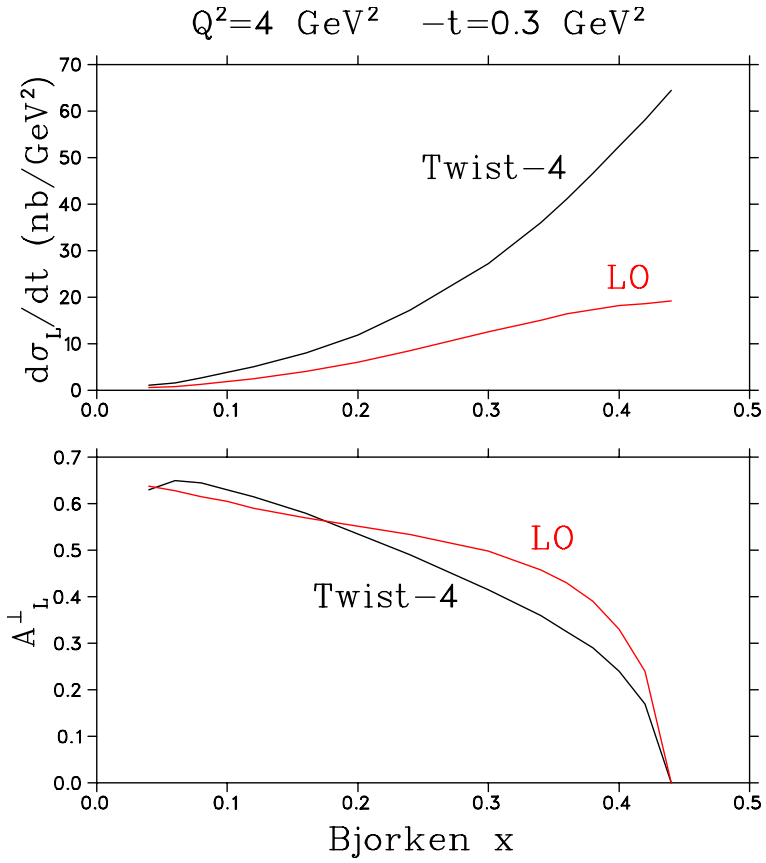

Figure 5: Calculation of the longitudinal photon transverse nucleon spin asymmetry including twist-four corrections by A. Belitsky [19] at $-t = 0.3$ GeV^2, Q^2=4 GeV^2. The red curves are the leading order calculation, while the black curves have twist-four power effects taken into account. While the cross section is very sensitive to these corrections, the transverse spin asymmetry is stable.

use of somewhat larger $-t$ data for pion form factor measurements, ultimately extending the Q^2-reach of pion form factor data acquired with JLab 12 GeV beam. Thus, measurements of the transverse single-spin asymmetry are a logical step in the support of the pion form factor program.

1.3 The Complementarity of Separated and Unseparated Asymmetry Measurements

The reaction of interest is ^{3}He$(e, e'\pi^-)p(pp)_{sp}$. The measurement of the transverse single-spin asymmetry requires the detection of the π^- in non-parallel kinematics. It is the component of the target polarization parallel to $\hat{q} \times \hat{p_\pi}$ that is important, and this direction is uniquely defined only in non-parallel kinematics.

Experimentally, the angle between the target polarization and the reaction plane, β, and the angle between the scattering and reaction planes, ϕ, are not independent. If the target polarization is at some angle, ϕ_s, relative to the scattering plane, then $\beta = \phi - \phi_s$.

The polarized nucleon cross section can be expressed [15, 16] in terms of these variables as:

$$
\begin{aligned}
d\sigma_{UT}(\phi,\phi_s) = \sum_k d\sigma_{UT_k}(\phi,\phi_s) \; = -\frac{P_\perp \cos\theta_q}{\sqrt{1-\sin^2\theta_q \sin^2\phi_s}} \Big[\; & \sin\beta \; \mathrm{Im}(\sigma_{++}^{+-} + \epsilon\sigma_{00}^{+-}) \\
& + \; \sin\phi_s \; \sqrt{\epsilon(1+\epsilon)} \; \mathrm{Im}(\sigma_{+0}^{+-}) \\
& + \; \sin(\phi+\phi_s) \; \frac{\epsilon}{2} \; \mathrm{Im}(\sigma_{+-}^{+-}) \\
& + \; \sin(2\phi-\phi_s) \; \sqrt{\epsilon(1+\epsilon)} \; \mathrm{Im}(\sigma_{+0}^{-+}) \\
& + \; \sin(3\phi-\phi_s) \; \frac{\epsilon}{2} \; \mathrm{Im}(\sigma_{+-}^{-+}) \; \Big],
\end{aligned}
\tag{8}
$$

where the $\cos\theta_q$ factor is needed to convert the target $P_\perp$ relative to the lepton beam to that relative to the virtual photon (in accordance with the Trento convention), and much smaller factors proportional to $\sin\theta_q$ have been neglected for clarity. The σ_{mn}^{ij} correspond to nucleon polarizations $ij = (+\frac{1}{2}, -\frac{1}{2})$ and photon polarizations $mn = (+1, 0, -1)$, and $\sigma_T = \frac{1}{2}(\sigma_{++}^{++} + \sigma_{++}^{--})$, $\sigma_L = \sigma_{00}^{++}$ are the usual unpolarized transverse and longitudinal cross sections.

From the above equation, it is clear that to extract $A_L^\perp$ it is necessary to first isolate the $\sin\beta$ Fourier component of the polarized nucleon cross section. Once that has been accomplished, one must then separate the desired σ_{00}^{+-} term from the σ_{++}^{+-} term via a Rosenbluth-type separation. All of the other polarized terms can be distinguished from their azimuthal dependences, without need of a Rosenbluth separation [15].

It has not yet been possible to perform an experiment to measure $A_L^\perp$. The conflicting experimental requirements of transversely polarized target, high luminosity, L–T separation, and closely controlled systematic uncertainty, make this an exceptionally challenging observable to measure. The SHMS+HMS is the only facility with the necessary resolution and systematic error control to allow a measurement of $A_L^\perp$. However, the beamtime required to do a good measurement with current polarized target technology is in the range of 10^3 days. To minimize the beamtime required, PR12-12-005 [4] proposed the use of a next generation, externally polarized, continuous flow, high luminosity ^{3}He target based on a large volume polarizer and compressor developed at the University of New Hampshire. The science case for this measurement was favorably reviewed by PAC39, and they encouraged the continued development of the target technology. Although the New Hampshire group is making continued progress on the development of the target, there is no timeline for its actual implementation at Jefferson Lab.

The most closely related measurement, of the transverse single-spin asymmetry in exclusive π^+ electroproduction without an L–T separation, was published by the HERMES Collaboration in 2010 [3]. Their data were obtained for average values of $\langle x_B \rangle = 0.13$, $\langle Q^2 \rangle = 2.38$ GeV^2 and $\langle t' \rangle = -0.46$ GeV^2, subject to the criterion $W^2 > 10$ GeV^2. The six Fourier amplitudes in terms of the azimuthal angles ϕ, ϕ_s of the pion-momentum and proton-polarization vectors relative to the lepton scattering plane were determined. Of these, at leading twist only the $\sin\beta_{UT}$ Fourier amplitude receives a contribution from longitudinal photons. If one assumes that longitudinal contributions dominate, these $A_{UT}^{sin(\phi-\phi_s)}$ values can be compared to GPD models for $\tilde{E}$, $\tilde{H}$.

Because transverse photon amplitudes are suppressed by $1/Q$, at very high Q^2 it is safe to assume that all observed meson production is due to longitudinal photons. At the lower Q^2 typical of the JLab and HERMES programs, however, this is not the case. Handbag-approach calculations by Goloskokov and Kroll [13] indicate much of the unseparated cross section measured by HERMES [3] is due to contributions

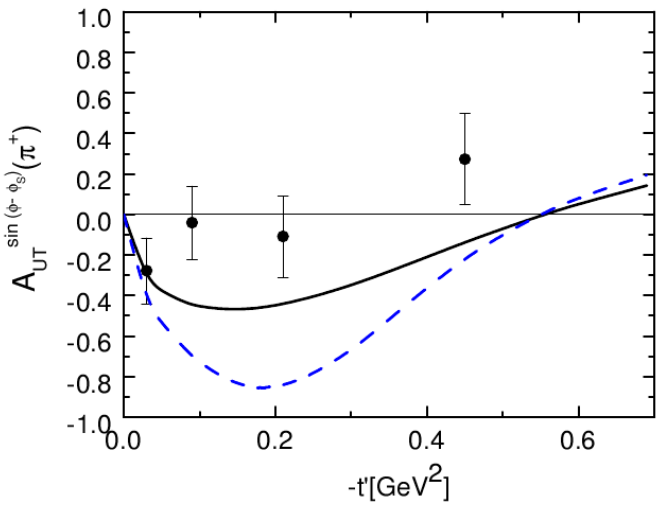

Figure 6: Predictions by Goloskokov and Kroll for the $\sin(\phi-\phi_s)$ moment of A_{UT} in the handbag approach, in comparison to the data from HERMES at $Q^2 = 2.45$ GeV^2, $W = 3.99$ GeV. Please note that the HERMES data follow the Trento convention, while the Eqns. 6, 7 and Figs. 4, 5 do not, leading to a normalization difference of $-\pi/2$ [16]. The independent variable is $-t' = |t - t_{min}|$. Dashed line: contribution from longitudinal photons only. Solid line: full calculation including both transverse and longitudinal photons. This figure is taken from Ref. [13].

from transversely polarized photons. In addition, there are contributions to $A_{UT}^{sin(\phi-\phi_s)}$ from the interference between two amplitudes, both for longitudinal photons, as well as transverse photons [15]. At the amplitude level, the transverse suppression is given by μ/Q, where $\mu \sim 2$ GeV is a mass parameter given by the pion mass enhanced by the large ratio between the pion mass and the sum of the u and d current quark masses (chiral condensate). For experimentally accessible Q^2, hardly any suppression of the twist-3 contribution is expected. As indicated in Fig. 6, the contribution from transverse photons tends to make the asymmetry smaller. At the HERMES kinematics, the dilution caused by transverse photons is about 50%. Although the observed unseparated asymmetry is small, the HERMES data are consistent with GPD models based on the dominance of $\tilde{E}$ over $\tilde{H}$ at low $-t'$, due to the pion pole. An improved measurement of the transverse target spin asymmetry, in particular the $\sin(\phi - \phi_S)$ modulation, is clearly a high priority.

A run-group proposal concurrent with the SoLID transversely polarized ^{3}He SIDIS experiment allows for an unseparated asymmetry measurement to be obtained on a sooner timescale than the Hall C measurement. In comparison to the HERMES measurement, the experiment proposed here will probe higher Q^2 and x_B, with much smaller statistical errors over a wider range of $-t$. SoLID will allow the first measurement for $Q^2 > 4$ GeV^2, where GPD-based calculations are expected to apply. Thus, the measurements should be more readily interpretable than those from HERMES. Similar measurements using CLAS-12 and a transversely polarized ^{1}H target have been discussed previously [23], but this measurement will allow for smaller statistical uncertainties, due to SoLID's higher luminosity capabilities.

Handbag model calculations by Goloskokov and Kroll [24] shed further light on the expected asymmetry dilution. The bottom panel of Fig. 7 shows their predictions for the cross section components in exclusive charged pion production. Although their calculations tend to underestimate the σ_L values measured in the JLab $F_\pi - 2$ experiment [26], their model is in reasonable agreement with the unseparated cross sections [13].

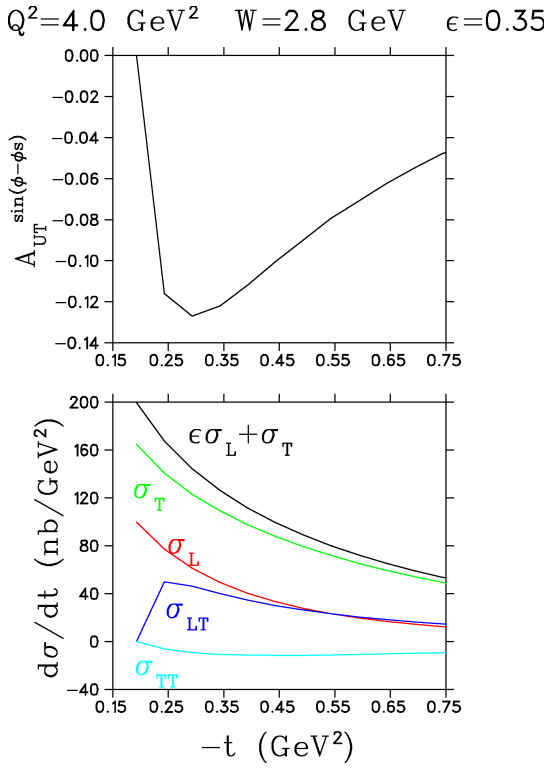

Figure 7: Calculation of the cross section components and $\sin(\phi - \phi_s)$ moment of the transverse nucleon spin asymmetry A_{UT} in the handbag approach by Goloskokov and Kroll [24] for kinematics similar to those in Fig. 5. Our measurement will be at higher $0.55 < \epsilon < 0.75$ than the $\epsilon = 0.35$ kinematics of this figure, so the dilution in the asymmetry will be significantly less.

They predict significant transverse contributions for JLab kinematics. A comparison of the unseparated asymmetry at $-t = 0.3$ GeV^2, $x_B = 0.365$ in Fig. 7 with the separated longitudinal asymmetry at the same values of x_B, $-t$ in Fig. 5 indicates a substantial dilution of the unseparated asymmetry due to transverse photon contributions, similar to that observed in Fig. 6.

In addition to allowing a measurement at $Q^2 > 4$ GeV^2, a measurement by SoLID of $A_{UT}^{sin(\phi-\phi_s)}$ will cover a fairly large range of $-t$, allowing the asymmetry to be mapped over its full range with good statistical uncertainties – from its required zero-value in parallel kinematics, through its maximum, and then back to near-zero or even positive at larger $-t$. The shape of the asymmetry curve versus $-t$, as well as its maximum value, are critical information for comparison to GPD-based models.

1.4 Motivation for and Status of the other Fourier Azimuthal Components

An important point is that any model that describes exclusive pion production will need to describe not only the leading-twist Fourier amplitude $A_{UT}^{sin(\phi-\phi_s)}$, but also the other contributions to the target-spin azimuthal asymmetry listed in Eqn. 8, providing additional GPD model constraints. Like HERMES, we plan to determine the full set of asymmetries from their azimuthal modulations,

$$A(\phi, \phi_s) = \frac{d\sigma_{UT}(\phi, \phi_s)}{d\sigma_{UU}(\phi)} = -\sum_k A_{UT}^{\sin(\mu\phi+\lambda\phi_s)_k} \sin(\mu\phi + \lambda\phi_s)_k, \tag{9}$$

where $d\sigma_{UU}$ is the unpolarized nucleon cross section in terms of the well-known L, T, LT and TT response functions. These asymmetries include all five terms listed in Eqn. 8, plus a very small $\sin(2\phi + \phi_s)$ term proportional to $\sin\theta_q$ not listed there.

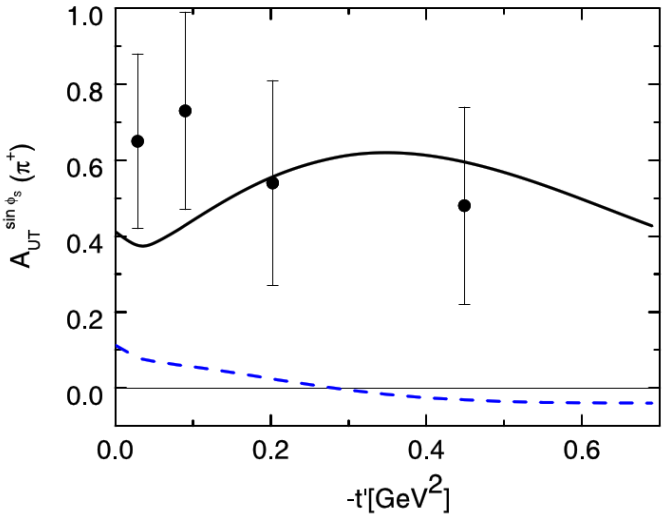

Figure 8: Data from HERMES for the $\sin(\phi_s)$ moment with a transversely polarized target at $Q^2 = 2.45$ GeV^2, $W = 3.99$ GeV. The solid line is the prediction of the handbag calculation by Goloskokov and Kroll; the dashed line is obtained disregarding the twist-3 contribution. This figure is taken from Ref. [13].

While most of the theoretical interest and the primary motivation of our experiment is the target asymmetry proportional to $\sin\beta$, there is growing interest in the $\sin(\phi_S)_{UT}$ asymmetry, as it may be interpretable in terms of the transversity GPDs. Independent of a specific dynamical interpretation (e.g. the handbag approach), the $A_{UT}^{sin(\phi_S)}$ asymmetry will say something on the strength of the contributions from transverse photons at small $-t$:

$$A_{UT}^{sin(\phi_S)} \sim \mathrm{Im}[M^*_{0+++}M_{0-0+} - M^*_{0-++}M_{0+0+}], \tag{10}$$

where the helicities are in the order: pion neutron photon proton [13]. In contrast to the $\sin(\phi - \phi_S)$ modulation, which has contributions from LL and TT interferences, the $sin(\phi_s)$ modulation measures only the LT interference. The first term is proportional to t', as is forced by angular momentum conservation, while the second one is not forced to vanish [24]. Indeed, HERMES measured the $\sin(\phi_s)$ modulation to be large and apparently nonzero at $-t' = 0$ (Fig. 8). Hence, both the amplitudes M_{0-++} and M_{0+0+} must be large, giving the first clear signal for strong contributions from transversely polarized photons at rather large values of W and Q^2 [13]. This is very interesting in its own right.

A calculation for the kinematics of this experiment by S.V. Goloskokov and P. Kroll [13, 24, 25] for the amplitudes of the five azimuthal modulations listed in Eqn. 8 is shown in Fig. 9. It clearly shows that the two asymmetries of greatest physics interest dominate, while the other asymmetries are much smaller. This is consistent with the HERMES result, which found the four asymmetries $\sin(2\phi - \phi_s)$, $\sin(phi + \phi_s)$, $\sin(3\phi - \phi_s)$, $\sin(2\phi + \phi_s)$, to be mostly consistent with zero over the measured t range [16]. This is good news, as large expected values for these asymmetries would complicate the extraction of the most-valued Fourier components.

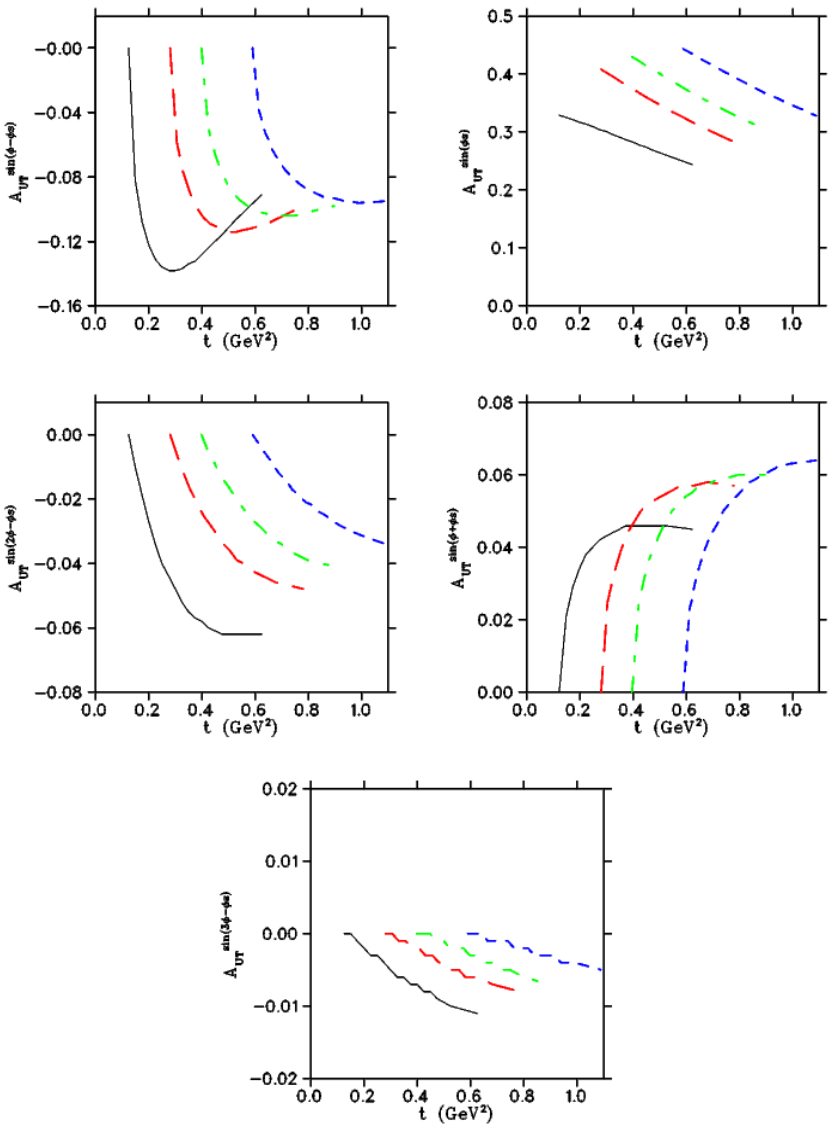

Figure 9: $\sin(\mu\phi + \lambda\phi_s)_k$ moments of the transverse nucleon spin asymmetry A_{UT} calculated in the handbag approach by Goloskokov and Kroll [24] for the kinematics of this experiment. Solid black: Q^2 = 4.107 GeV^2, W =3.166 GeV; Long-dash red: Q^2 = 5.138 GeV^2, W =2.796 GeV; Dash-dot green: Q^2 = 6.049 GeV^2, W =2.718 GeV; Short-dash blue: Q^2 = 6.894 GeV^2, W =2.562 GeV.

In the longer term, the measurement presented in this proposal is important preparatory work for future measurements at the EIC. The Electron-Ion Collider is optimized for transverse single spin asymmetry measurements such as these, and the ability to have both polarized ^{3}He and proton beams will allow $A_{UT}^{sin(\phi-\phi_s)}$ to be directly compared for the $\vec{n}(e,e'\pi^-)p$ and $\vec{p}(e,e'\pi^+)n$ reactions, without target dilution, over a broad kinematic range. In the meantime, the proposed measurement with SoLID is our best short-term opportunity to considerably advance over the pioneering HERMES data.

2 Experimental Method

We propose to carry out the $^3He(e,e'\pi^-)p(pp)_{sp}$ measurement using the Solenoidal Large Intensity Device (SoLID [2]), in parallel with the already approved experiment, E12-10-006 [1], which will measure Semi-Inclusive Deep-Inelastic Scattering (SIDIS). Our discussion will concentrate on the region of clearest physics interpretation (Q^2 >4 GeV^2), even through lower Q^2 events will also be contained in the experimental data-set.

There are two SoLID configurations, called SoLID-SIDIS and SoLID-PVDIS. Besides E12-10-006, two SIDIS experiments, E12-11-007 [27] and E12-11-108 [28], along with the J/ψ experiment (E12-12-006 [29]), will use the SoLID-SIDIS configuration as well. All of these experiments have been approved with A or A-rating. In addition, two "bonus-run" experiments, E12-10-006A [30] and E12-11-108A [31], have also been approved to run in parallel with the SIDIS experiments. The SoLID-PVDIS configuration is for the Parity Violation in Deep Inelastic Scattering (PVDIS) [32].

In order to assure a clean measurement of exclusive π^- production, it is required to detect the recoil proton from the $\vec{n}(e,e'\pi^-)p$ reaction. The existing SoLID detectors already have the capabilities of detecting protons from 8° up to 24°, while the main proton events from the DEMP process can cover 0° up to 50°. The experiment will use exactly the same setup and online production trigger as E12-10-006, which is the coincidence of electron triggers and hadron triggers from SoLID. We will perform the offline analysis to identify the recoil protons from DEMP and form the triple coincidence events together with electrons and π^- provided by SIDIS triggers. The discussion of proton detection will be given in Section 2.3.

2.1 Transversely Polarized ^{3}He Target

Target	^{3}He
Length	40 cm
Target Polarization	∼60%
Target Spin Flip	≤20 mins
Target Dilution	90%
Effective Neutron	86.5%
Target Polarimetry Accuracy	∼ 3%

Table 1: Key Parameters of the ^{3}He target.

The proposed measurement will utilize the same polarized ^{3}He target as E12-10-006 [1]. Such a target was successfully employed in E06-110, a 6 GeV SIDIS experiment in Hall A. A wide range of experiments have utilized polarized ^{3}He as an effective neutron target over a wide range of kinematics. And over the past decades several authors have calculated the effective neutron polarization in ^{3}He using three-nucleon wave functions and various models of the $N-N$ interaction [33]. These are now well established, and the error introduced by uncertainty in the wave functions are small.

Other nuclear effects which can influence the experimental asymmetry for a neutron bound inside ^{3}He include Fermi motion, off-shell effects, meson exchange currents, delta isobar contributions and π^- final state interactions. The exclusive nature of the process, the selected kinematics such as high Q^2, large recoil

momentum and a complete coverage of the azimuthal angle ϕ ensures that corrections due to these nuclear effects will be small and can be modeled effectively.

The ^{3}He polarization direction is held by three sets of Helmholtz coils with a 25 Gauss magnetic field. Both the transverse and longitudinal directions can be provided by rotating the magnetic field. The ^{3}He gas, with density of about 10 atm (at 0°C), is stored in a 40 cm target cell made of thin glasses. With a 15 μA electron beam, the neutron luminosity can be as high as 10^{36} cm^{-2}s^{-1}. In-beam polarization of 60% was archived during the E06-110 experiment. Two kinds of polarimetry, NMR and EPR, were used to measure the polarization with relative 5% precision. We have plans to improve the accuracy of the measurement to reach 3%.

The target spin will be reversed for every 20 minutes by using the RF AFP technique. The additional polarization loss due to the spin reversal was kept at $< 10\%$, which has been taken into account in the overall 60% in-beam polarization. A new method for spin reversal using field rotation has been tested and was able to eliminate the polarization loss. Such an improvement will enable us to perform the spin-reversal in few minutes to reduce the target-spin-correlated systematic errors. The key parameters of the ^{3}He target are summarized in Table 1.

A collimator, similar to the one used in the E06-110, will be placed next to the target cell window to minimize the target cell contamination and to reduce the event rate. Several calibration targets will also be installed in this target system, including a multi-foil ^{12}C for optics study, a BeO target for beam tuning, and a reference target cell for dilution study and other calibration purposes.

2.2 SoLID Spectrometer and Detectors

The solenoid magnet for SoLID will be based on the CLEO-II magnet built by Cornell University. The magnet is 3 meters long with an outer diameter of 3 meters and an inner diameter of 1 meter. The field strength is greater than 1.35 Tesla, with an integrated BDL of 5 Tesla-meters. The fringe field at the front end after shielding is less than 5 Gauss. In the SIDIS-configuration, the CLEO-II magnet provides 2π acceptance in the azimuthal angle (ϕ) and covers polar angle (θ) from 8° up to 24°. The momentum acceptance is between 0.8 and 7.5 GeV/c for electrons and for hadrons, the momentum can be lower depending on the trigger efficiency. The momentum resolution is about 2%.

The layout of the SoLID detectors in the SIDIS-configuration is shown in Fig. 10. The detector system is divided into two regions for the forward-angle (FA) detection and the large-angle (LA) detection. Six tracking chambers based on Gas Electron Multipliers (GEM) will be used for charged particle tracking in the forward-angle region, and the first four of them will be shared by the large-angle region. In each region, a Shashlyk-type sampling EM calorimeter (LAEC or FAEC) will measure the particle energy and identify electrons from hadrons. A scintillator-pad detector (LASPD or FASPD) will be installed in front of each EC to reject photons and provide timing information. The forward-angle detectors will detect both the electrons and hadrons (mainly $\pi^{\pm}$). A light-gas Čerenkov detector (LGC) and a heavy-gas Čerenkov detector (HGC) will perform the $e/\pi^{\pm}$ and $\pi^{\pm}/K^{\pm}$ separation, respectively. The Multi-gas Resistive Plate Chamber (MRPC) will provide a precise timing measurement and serve as a backup of the FASPD on photon rejection. A more detailed discussion of the design, simulation, prototype-test of each detector is given in the SoLID preliminary conceptual design report (pCDR) [2].

Table 2 summarizes the key parameters of the detector system in the SIDIS configuration for both the

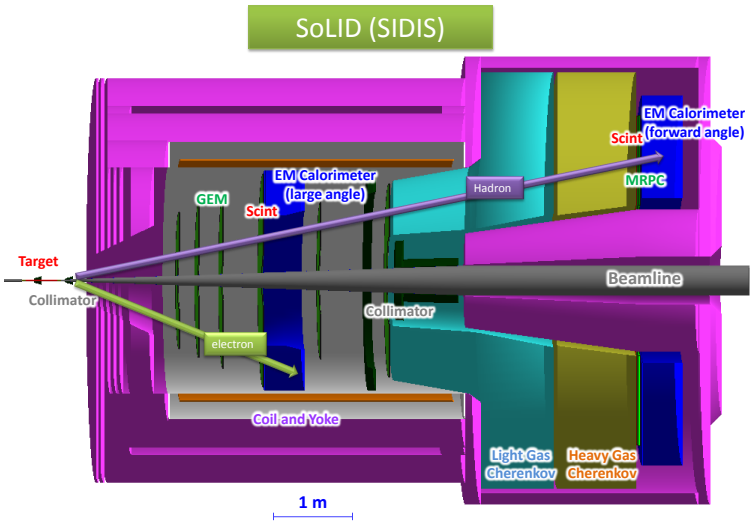

Figure 10: The Detector Layout of the SoLID-SIDIS configuration. The detector system includes six Gas Electron Multiplier (GEM) planes for charged particle tracking, two Scintillator Pad Detectors (SPD) followed by two Shashlyk sampling EM Calorimeters (EC) for energy measurement and particle identification, a Light Gas Čerenkov Detector (LGC) for e-$\pi^{\pm}$ separation, a Heavy Gas Čerenkov Detector (HGC) for $\pi^{\pm}$-$K^{\pm}$ separation, as well as a Multi-gap Resistive Plate Chamber (MRPC) for timing measurement. The first four GEM trackers, the first SPD (i.e. LASPD) and EC (i.e. LAEC) form the large-angle detection system for electron measurement. The forward-angle detection system, to measure electron and hadrons, is composed of all six GEM trackers, LGC, HGC, MRPC, the second SPD (i.e. FASPD) and the second EC (FAEC).

SIDIS and DEMP measurements.

2.3 Recoil Proton Identification

The cleanest way to identify the DEMP events is to detect all particles in the final state. The SoLID-SIDIS detector system has the capability of measuring electrons and pions, while protons can be isolated from other charged particles by using the time-of-flight (TOF) information. The TOF is provided by the timing detectors, including the MRPC and FASPD at the forward-angle detection region, and the LASPD at the large-angle detection region.

We examined the requirement of the timing resolution on these detectors by looking at the time difference between electrons and other heavier charged particles when they reach these detectors with the same momentum and flight path. As shown in the next section, the good protons from the DEMP reaction carry momenta from 0.3 GeV/c up to 1.2 GeV/c with angles from 0° to 50°. The FA-MRPC covers angles from 8° to 14.8°, and the angular range of the LASPD is from 16° to 24°. Hence we simulated events of electrons, pions, kaons and protons with the momentum from 0.3 GeV/c up to 1.2 GeV/c, and calculated the time when they reach two different detectors with linear trajectories and at fixed angles.

The results are shown in Fig. 11. To clearly identify two types of charged particles with the same momentum, we normally require the timing difference between two particles to be larger than 5 times of the overall timing resolution, while the SoLID timing detectors can reach the resolution in the range of 150 ps down to 50 ps. At the FA-MRPC, which is more than 7 meters from the target, protons come 3 ns later than

Experiments	SIDIS	DEMP
Reaction channel	$\vec{n}(e, e'\pi^{\pm})X$	$\vec{n}(e, e'\pi^{-}p)$
Target	^{3}He	same
Unpolarized luminosity	$\sim 10^{37}$ cm^{-2}s^{-1} per nucleon	same
Momentum coverage	0.8-7.5 (GeV/c) for e^-,$\pi^{\pm}$	same 0.3 1.2 (GeV/c) for protons
Momentum resolution	$\sim$2%	same
Azimuthal angle coverage	0° 360°	same
Azimuthal angle resolution	5 mr	same
Polar angle coverage	8°-24° for e 8°-14.8° for $\pi^{\pm}$	same same 8°-24 ° for p in SoLID 24°-50° for p with recoil detector
Polar angle resolution	0.6 mr	same
Target Vertex resolution	0.5 cm	same
Energy resolution on ECs	5%$\sim$10%	same
Trigger type	Double Coincidence $e^- + \pi^{\pm}$	same (online) Triple Coincidence $e^- + \pi^- + p$ (offline)
Expected DAQ rates	<100 kHz	same (online)
Main Backgrounds	^{3}He(e,e'K$^{\pm}$/π^0)X Accidental Coincidence	^{3}He(e,e'$\pi^{\pm}$/K$^{\pm}$)X Accidental Coincidence
Key requirements	Radiation hardness Kaon Rejection DAQ	Proton Detection Exclusivity Timing Resolution

Table 2: Summary of Key Parameters for DEMP Measurement compared with SIDIS Experiments.

kaons, even at the highest momenta in the DEMP reaction. Hence, protons will be easily distinguished from other lighter particles. At the LA-SPD, which is about 3 meters away from the target, the time difference between protons and kaons is still more than 1 ns, which doesn't demand precise timing resolution.

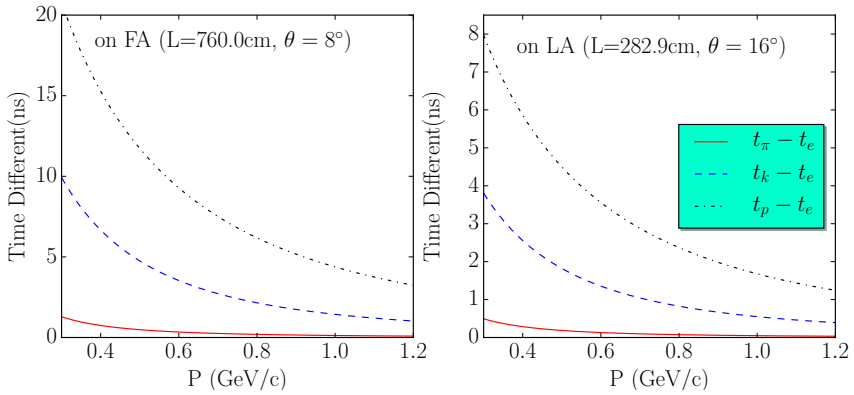

Figure 11: The time differences (in ns) between electrons and other charged particles, i.e. pions (red solid line), kaons (blue dashed line) and proton (black dash-dotted line), and their distributions as functions of particles' momentum at two different timing detectors, including the forward-angle (FA) MRPC and the large-angle (LA) SPD.

In general, the misidentified proton events can be mostly removed by cutting on the reconstructed missing quantities, e.g. angles, momenta and masses. The residual background will also be largely suppressed in the target-spin asymmetry extraction.

2.4 Trigger Design

In E12-10-006, the online production trigger will be the double-coincidence of the scattered electrons and hadrons. One will use the particle identification detectors, such as LGC, HGC and ECs, during the offline analysis to select $\pi^{\pm}$ out from other hadrons. The DEMP events will be identified with the triple-coincidence of the scattered electron, π^- and proton, while the proton identification has been discussed above. We will use the same online trigger as the SIDIS one, and hence the new experiment will share exactly the same data-set as E12-10-006. The actual design of the SIDIS triggers will be far more complicated, and the detailed discussion of the trigger and DAQ designs is given in the SoLID pCDR [2].

3 Projected Results

To perform the simulation study and obtain the projected results, we developed a DEMP generator, as discussed in Appendix-A, and used it to generate events within a kinematic phase space slightly larger than the SoLID-SIDIS acceptance. The Fermi motion of the neutron in ^{3}He, multiple scattering of the final state particles, and energy lose due to the ionization, the radiative effects and so on have been taken in account in this generator. Then for every detected article in each event, we added the acceptance profiles obtained from the GEANT4 simulation with the SoLID-SIDIS configuration and smear the momenta and angles of the final state particles by the detector resolutions based on current knowledge of tracking reconstruction study. To better simulate the real experimental conditions, we generated two sets of data with the target polarization up and down, respectively.

3.1 Kinematic Coverage

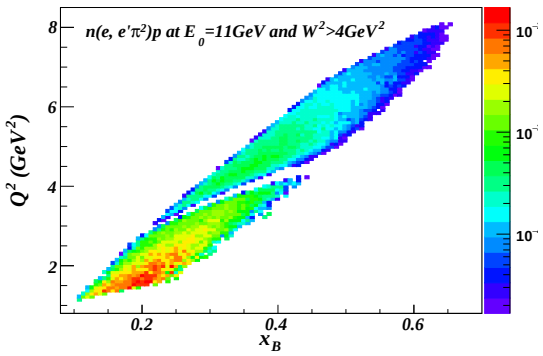

Figure 12: The kinematic coverage at 11 GeV within the SoLID acceptance. A cut W^2 >4 GeV^2 was applied.

The kinematic coverage in Q^2 vs. x_B is shown in Fig. 12, using the existing SoLID detectors to detect electrons, pions and protons at $8^\circ \sim 24^\circ$. These distributions were weighted by the DEMP unpolarized cross sections and the SoLID acceptance profiles for electrons, pions and protons. A cut $W^2 > 4\ GeV^2$ was also applied to exclude non-DIS events.

Fig. 13 shows the momentum and angular acceptance of electrons, π^- and protons which form the DEMP events and can be detected with the SoLID detectors. Cuts of $Q^2 > 4$ GeV^2 and W^2 >4 GeV^2 were applied since this is the region of greatest physics interest. The recoil protons shown in Fig. 13 have low momenta ranging from 0.3 GeV/c up to 1.5 GeV/c and distributes in both the large- and forward-angle regions. angle.

3.2 Estimated Rates

Table 3 lists the triple-coincidence rate of the DEMP events after applying cuts on . The rates were calculated with the simulated events weighted by the target luminosity, the SoLID acceptances and unpolarized cross sections. The "raw" rates are not corrected by the beam and target polarization, target dilution and so on. Our conservatively estimated rate is around 4.22 Hz at Q^2 >1 GeV^2, or 0.20 Hz at Q^2 >4 GeV^2. For

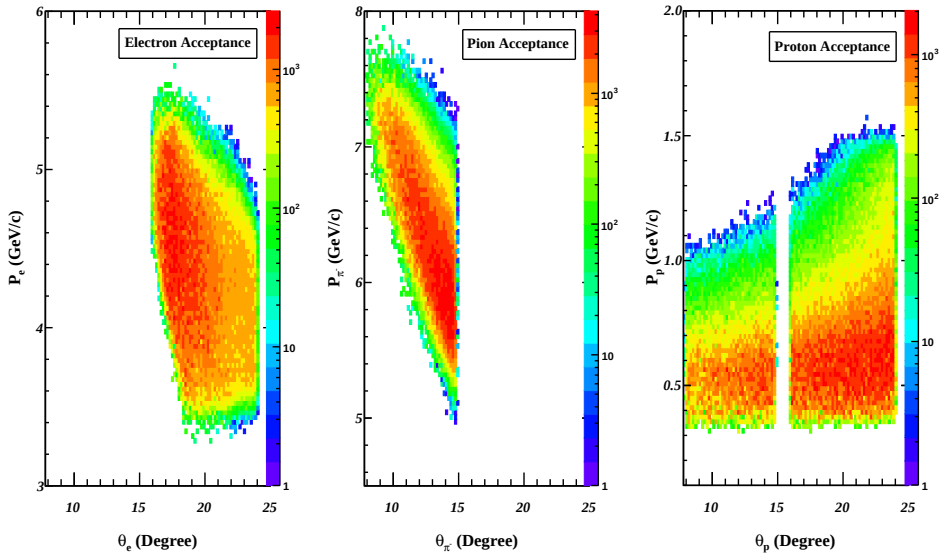

Figure 13: The acceptance of the momenta and polar angles. The top, middle and bottom plots are for electrons, π^- and protons, respectively. Cuts of $Q^2 > 4$ GeV^2 and $W^2 > 4$ GeV^2 were applied.

$Q^2 > 1$ GeV^2	$Q^2 > 4$ GeV^2
DEMP: $\vec{n}(e, e'\pi^-p)$ Triple-Coincidence (Hz)	
4.95	0.48
SIDIS: $\vec{n}(e, e'\pi^-)X$ Double-Coincidence (Hz)	
1424.62	35.77

Table 3: Triple-Coincidence rates for DEMP events compared with the SIDIS rates. A cut $W^2 > 4$ GeV^2 was applied. The online production trigger will be the SIDIS double-coincidence trigger of which rates are also given.

comparison, the table also gives the SIDIS rate which will be the online production trigger rates and is the main background of the DEMP events.

3.3 Asymmetry Projections

The proposed experiment will run in parallel with E12-10-006, which has already been approved to run 48 days at E_0=11 GeV. As shown in Fig. 14, we defined 7 $-t$ bins of which the boundaries are defined by the array:

$$-t[8] = [0.0, 0.15, 0.25, 0.35, 0.45, 0.55, 0.75, 1.10] \quad \text{(in GeV}^2\text{)} \tag{11}$$

The number of events ($N_i^{\uparrow\downarrow}$) in the ith bin is calculated from the total simulated events after applying cuts on important kinematic variables, e.g. $Q^2 > 4$ GeV^2, $W > 2$ GeV, $0.55 < \epsilon < 0.75$ and $-t_{min} < -t < -t_{max}$. Two simulated data sets with target polarization up and down follow exact the same cuts and binning. As shown in Eqn. 12, each event surviving the cuts is then weighted by the polarized cross section, together with the acceptance of the electron, pion and proton. $N_i^{\uparrow\downarrow}$ is further corrected by the phase-space factor (PSF) defined in the event generator, the total number of randomly generated events (N_{gen}), beam-time

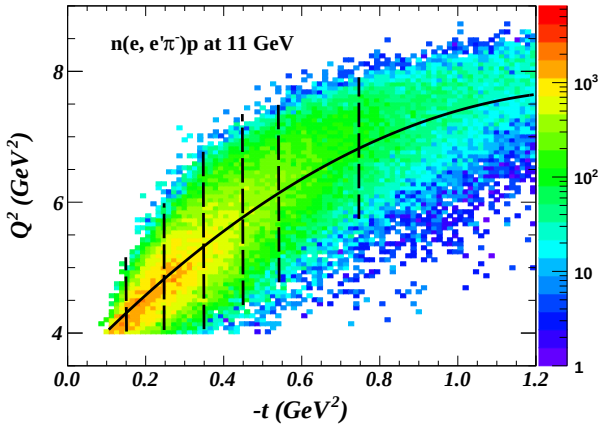

Figure 14: Q^2 vs. $-t$ where the black dashed lines specify the boundaries of 7 $-t$ bins and the black dash-dot lines indicate the additional two Q^2 bins.

(T), the target luminosity ($L = 10^{36}$ cm^{-2}s^{-1}), and the overall detector efficiency (ϵ_{eff}):

$$N_i^{\uparrow\downarrow} = \Big(\sum_{j \in i-bin} \sigma_j^{\uparrow\downarrow} \cdot A_j^e \cdot A_j^{\pi^-} \cdot A_j^p \Big) \cdot (PSF/N_{gen}) \cdot T \cdot L \cdot \epsilon_{eff}, \tag{12}$$

where j is the jth event in the ith bin, $\sigma_j^{\uparrow\downarrow}$ is the cross section of the jth event with the target polarization up or down. $A_j^{e(\pi^-,p)}$ is the acceptance weight of the electron (pion, proton) in this event. The detector efficiency, ϵ_{eff}, is approximately fixed at 85% as was used in SIDIS proposals. $N_i^{\uparrow\downarrow}$ corresponds to the raw experimental count of electrons scattering on neutrons in ^{3}He after taking into account the target polarization ($P \sim 60\%$), the effective polarization of neutrons ($\eta_n \sim 0.865$), and the dilution effect from other reaction channels when electrons scattering on ^{3}He ($d \sim 0.9$).

In addition, we further divide each $-t$-bin into two Q^2 bins with similar statistics, as indicated in Fig. 14. By doing that, we are able to examine the Q^2-dependence of the asymmetries, and also check the model dependence of the other corrections that are directly related to the values of Q^2.

With the numbers of simulated events in each bin for two anti-parallel target polarizations, one is able to reconstruct the average target single-spin asymmetry in that bin, which is identical to the experimental extracted asymmetry:

$$< A_{UT} >= \frac{1}{P \cdot \eta_n \cdot d} \frac{N^\uparrow - N^\downarrow}{N^\uparrow + N^\downarrow}. \tag{13}$$

The statistical error of the target single spin asymmetry (A_{UT}) in each bin can be given as:

$$\delta A_{UT} = \frac{1}{P \cdot \eta_n \cdot d} \sqrt{\frac{1 - (P \cdot < A_{UT} >)^2}{N_i^\uparrow + N_i^\downarrow}}, \tag{14}$$

Shown in Eq. **??** in Section 1.4, A_{UT} can be further decomposed into six asymmetries with different azimuthal angular modulations:

$$\begin{aligned} A_{UT}(\phi, \phi_S) &= A_{UT}^{sin(\phi-\phi_S)} sin(\phi - \phi_S) + A_{UT}^{sin(\phi_S)} sin(\phi_S) \\ &+ A_{UT}^{sin(2\phi-\phi_S)} sin(2\phi - \phi_S) + A_{UT}^{sin(3\phi-\phi_S)} sin(3\phi - \phi_S) \\ &+ A_{UT}^{sin(\phi+\phi_S)} sin(\phi + \phi_S) + A_{UT}^{sin(2\phi+\phi_S)} sin(2\phi + \phi_S). \end{aligned} \tag{15}$$

In our generator, the first five different azimuthal modulations of A_{UT} are predicted with a phenomenological model as discussed in Appendix-A, and the last modulation is fixed to be zero as the model predicts a negligible asymmetry. As discussed in Section 1, two modulations, $A_{UT}^{sin(\phi-\phi_S)}$ and $A_{UT}^{sin(\phi_S)}$, are particularly interesting and are the main quantities this proposal aims to measure.

To demonstrate that the proposed measurement has the capability of extracting these two asymmetries, we adopted the procedure presented in the HERMES thesis [16] to extract all five asymmetries by using a unbinned maximum likelihood (UML) method. Compared with the regular extraction methods where the data in each -t bin are further binned into two dimensional (ϕ, ϕ_S) bins, the UML method can perform much better fitting when the statistics is limited.

The polarized cross sections with two target polarization directions are given approximately:

$$\sigma_{\uparrow} = \sigma_{UT}(\phi,\phi_S) = [1 + \frac{|P_T|}{\sqrt{1-sin^2(\theta_\gamma)sin^2(\phi_S)}} A_{UT}(\phi,\phi_S)] \cdot \sigma_{UU}(\phi) \tag{16}$$

$$\sigma_{\downarrow} = \sigma_{UT}(\phi,\phi_S+\pi) = [1 - \frac{|P_T|}{\sqrt{1-sin^2(\theta_\gamma)sin^2(\phi_S)}} A_{UT}(\phi,\phi_S)] \cdot \sigma_{UU}(\phi). \tag{17}$$

where $|P_T| = P \cdot \eta_n \cdot d$. Hence, the probability density function can be constructed as:

$$f_{\uparrow\downarrow}(\phi,\phi_S;\theta_k) = \frac{1}{C_{\uparrow\downarrow}}[1 \pm \frac{|P_T|}{\sqrt{1-sin^2(\theta_\gamma)sin^2(\phi_S)}} \sum_{k=1}^{5} \theta_k sin(\mu\phi + \lambda\phi_S)], \tag{18}$$

where θ_k, $k = 1-5$, are the values of asymmetries that can maximize the likelihood function. $C_{\uparrow\downarrow}$ is a normalization constant and is set to one as it is not important in the UML fitting. Here we have dropped out the sixth asymmetry which is zero. The UML function can be defined as:

$$L(\theta_k) = L_{\uparrow}(\theta_k) \cdot L_{\downarrow}(\theta_k) = \prod_{l=1}^{N_{MC}^{\uparrow}} [f_{\uparrow}(\phi_l,\phi_{S,l};\theta_k)]^{w_l^{\uparrow}} \cdot \prod_{m=1}^{N_{MC}^{\downarrow}} [f_{\downarrow}(\phi_m,\phi_{S,m};\theta_k)]^{w_m^{\downarrow}}. \tag{19}$$

where $w_l^{\uparrow} = \sigma_l^{\uparrow} \cdot A_l^e \cdot A_l^{\pi^-} \cdot A_l^p \cdot PSF/N_{gen} \cdot T \cdot L \cdot \epsilon_{eff}$, is the weight of the lth simulated event. It takes into account the fact that the Monte-Carlo events are generated uniformly, and it also includes the experimental conditions such as the acceptances of three particles and the detector efficencies. For the real experimental data, the weight will only takes into account the acceptance correction, detector efficiencies correction and other experimental related corrections. From Eq. 12, one has $N_i^{\uparrow} = (\sum_{l\in i-bin} w_l^{\uparrow})$. Note that $N_{MC}^{\uparrow} = (\sum_{l\in i-bin})$ is simply the total number of simulated events in the ith $-t$ bin without any weighting. In practice, we use the TMinuite package to minimize the following negative log-likelihood function:

$$-lnL(\theta_k) = -lnL_{\uparrow}(\theta_k) - lnL_{\downarrow}(\theta_k) = -\sum_{l=1}^{N_{MC}^{\uparrow}} w_l^{\uparrow} \cdot lnf_{\uparrow}(\phi_l,\phi_{S,l};\theta_k) - \sum_{m=1}^{N_{MC}^{\downarrow}} w_m^{\downarrow} \cdot lnf_{\downarrow}(\phi_m,\phi_{S,m};\theta_k). \tag{20}$$

Fig. 15 (Fig. 16) compare the distribution of $A_{UT}^{sin(\phi-\phi_S)}$ ($A_{UT}^{sin(\phi_S)}$) vs. $-t$ between values from the UML fitting and from the direct statistical averaged model calculations. Compared with the existing HERMES results (Fig. 6), the new measurement could provide more precision data to be directly compared with theoretical predictions. Extra binning on Q^2 enables us to study the Q^2-dependence of asymmetries as well as to constraint some corrections during the asymmetry extraction. The detailed information of each bin is listed in Table 4.

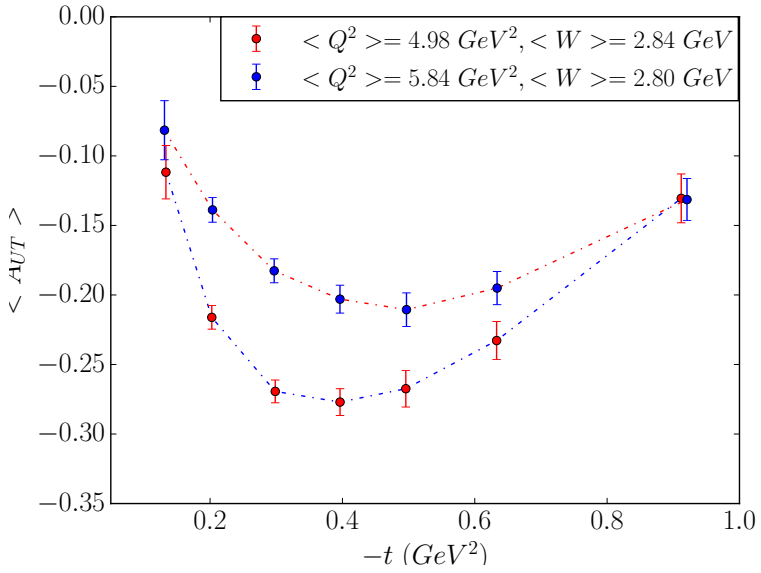

Figure 15: Projection of $A_{UT}^{sin(\phi-\phi_S)}$ as a function of $-t$ (directly compare with Fig. 6).

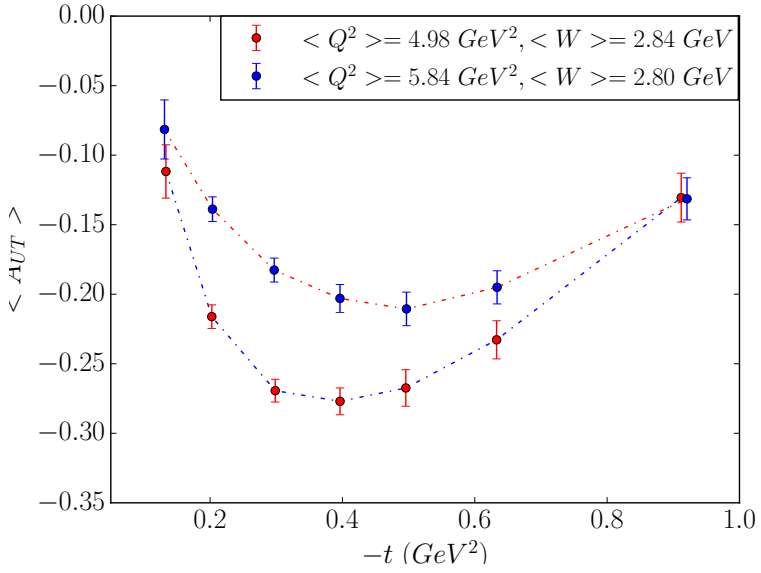

Figure 16: Projection of $A_{UT}^{sin(\phi-\phi_S)}$ as a function of $-t$ (directly compare with Fig. 6).

3.4 Missing Mass and Background

In the DEMP reaction on a neutron, all three charged particles in the final state, e^-, π^- and p, can be cleanly measured by the SoLID detector system. Hence, contamination from other reactions, including DEMP with other two protons in ^3He, can be greatly eliminated. The dominant background of the DEMP measurement comes from the SIDIS reactions of electrons scattering on the neutron and two protons in ^{3}He.

Q^2 bin-set#1							
	t-bin#1	t-bin#2	t-bin#3	t-bin#4	t-bin#5	t-bin#6	t-bin#7
$< -t >$	0.13	0.20	0.30	0.40	0.50	0.63	0.91
$< Q^2 >$	4.11	4.36	4.73	5.10	5.48	5.96	6.66
$< A_{UT} >$	-1.12×10^{-1}	-2.16×10^{-1}	-2.69×10^{-1}	-2.77×10^{-1}	-2.67×10^{-1}	-2.33×10^{-1}	-1.31×10^{-1}
δA_{UT}	1.92×10^{-2}	8.49×10^{-3}	8.18×10^{-3}	9.64×10^{-3}	1.32×10^{-2}	1.37×10^{-2}	1.76×10^{-2}
Q^2 bin-set#2							
	t-bin#1	t-bin#2	t-bin#3	t-bin#4	t-bin#5	t-bin#6	t-bin#7
$< -t >$	0.13	0.20	0.30	0.40	0.50	0.63	0.92
$< Q^2 >$	4.35	4.87	5.45	5.98	6.43	6.92	7.63
$< A_{UT} >$	-8.15×10^{-2}	-1.39×10^{-1}	-1.83×10^{-1}	-2.03×10^{-1}	-2.11×10^{-1}	-1.95×10^{-1}	-1.31×10^{-1}
δA_{UT}	2.20×10^{-2}	9.17×10^{-3}	8.91×10^{-3}	1.04×10^{-2}	1.25×10^{-2}	1.23×10^{-2}	1.57×10^{-2}

Table 4: Detailed information of projected bins from the new DEMP measurements with SoLID, while $< Q^2 >$ and $< -t >$ are in the unit of GeV^2. The data are divided into 14 $-t$ bins in both $-t$ (7 bins) and Q^2 (2 bins). The projected uncertainties are statistical only.

In addition to detecting the recoil protons, which should largely suppress most of background, we will also rely on reconstructing the neutron missing mass spectrum to ensure the exclusivity of the DEMP events. In SIDIS, however, the final states include the scattered electron, the hadrons ($\pi^{\pm}$, $K^{\pm}$ etc.), as well as the undetected target fragments which could contain protons. Hence, the SIDIS events will possibly leak into the DEMP missing mass spectrum.

We studied the contamination of the SIDIS events in the DEMP missing momentum and mass spectra. The SIDIS reactions, $p(e, e'\pi^-)X$ and $n(e, e'\pi^-)X$, were simulated with the same generator used for the SoLID-SIDIS proposals, and their rates were calculated by matching the acceptance of scattered electrons and pions with the ones in DEMP. We then fold the SoLID detector resolutions into the spectra. Based on the current tracking study, the SoLID-SIDIS system can provide a momentum resolution of $2\%/\sqrt{E}$, a polar angle resolution of 0.6 mrad, an azimuthal angle resolution of 5 mrad and a vertex target position of 0.5 cm. It is difficult to estimate what percentage of the SIDIS target fragments contain protons, so we assumed the target fragments ("X'') all contain one or more protons. Such an assumption likely results in the SIDIS background being significantly overestimated.

Fig. 17 shows a reconstruction of the missing momenta of both processes. One immediately sees that the missing momentum distributions of two processes are well separated. The SIDIS background can be largely rejected when we apply a cut, $P_{miss} < 1.0$ GeV/c.

We then reconstructed the missing mass spectra of the DEMP and SIDIS events w/ and w/o the missing momentum cuts, as shown in Fig. 18. Before applying the missing momentum cut, the SIDIS background overwhelms the DEMP peak (note that, however, the SIDIS rate is likely overestimated). After applying the cut, the DEMP peak dominates and the SIDIS background is largely suppressed. The total integrated SIDIS becomes 0.04Hz compared with the rate of DEMP rate (0.2Hz). If we consider the fact that not every "X'' in SIDIS contains a proton, the remaining background should be negligible.

Other random coincident background events will show up in the missing mass spectrum with more uniform distributions. We should be able to suppress most of them with tight missing momentum and missing mass cuts, and for these residuals that contaminate the real events, we are able to evaluate their asymmetries

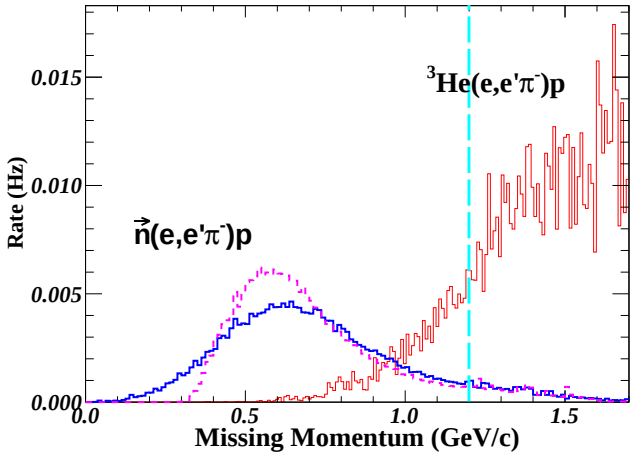

Figure 17: Missing momentum spectra of DEMP and SIDIS events in the worse scenario where we assume all SIDIS events contain protons in the final state. The missing momentum distributions are well separated between the two processes and one can apply a cut at $P_{miss} < 1.0$ GeV/c (indicated by the light-blue dashed line) to remove most of the SIDIS events.

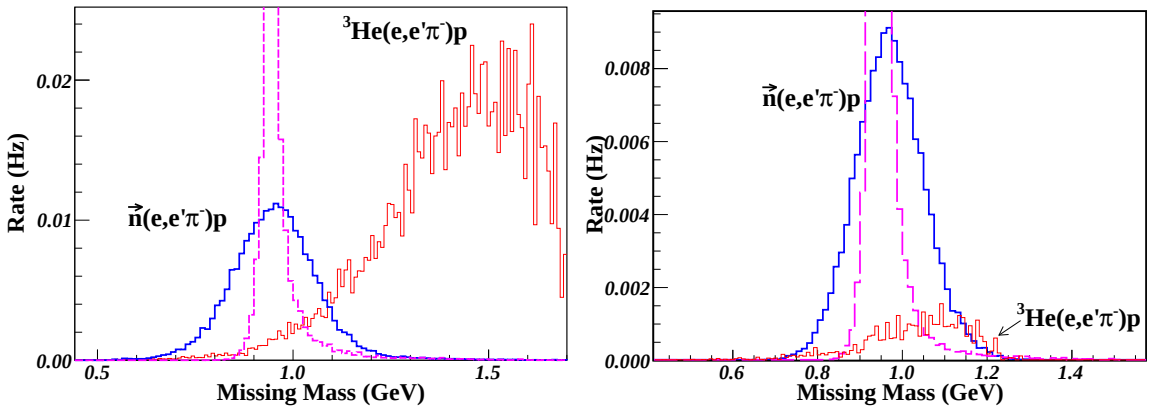

(a) Before cutting on missing momentum

(b) Before cutting on missing momentum

Figure 18: Missing mass spectra of DEMP and SIDIS events in the worse scenario where we assume all SIDIS events contain protons in the final state. Top (bottom) panel shows the missing mass distribution of DEMP events. The left (right) plot of each panel shows the background contamination from SIDIS events before (after) the missing momentum cut shown in Fig. 17. The broadening effect of the missing mass due to the Fermi motion and the energy loss is indicated by the magenta curve. The SIDIS background is already small compared with DEMP events before optimizing the cut. The actual SIDIS background should be much smaller, since we overestimated the SIDIS rate by assuming all target fragments "X"') in the SIDIS process contain protons.

if nonzero, and apply corrections on the real asymmetry values. In general, we expect to have a clean measurement of the DEMP process because all of the final particles being detected.

3.5 Systematic Uncertainties

The systematic errors are expected to be close to the ones given in the E12-10-006 proposal as well as in other SIDIS experiments with SoLID. The procedure of extracting DEMP asymmetries is also expected to

Sources	**Relative Value**
Beam Polarization	2%
Target Polarization	3%
Dilution Factor	1%
Nuclear Effect	$< 4\%$
Acceptance	3%
Radiation Correction	2%
Background Contamination	$< 5\%$

Table 5: Expected systematic errors.

be similar to the SIDIS asymmetry extraction. The contamination of background should be well controlled by the proton detection and cuts on missing momenta and mass. However, to be conservative, we quote the overall systematic errors of background contamination to be 5% level. Here we list several major sources of systematic uncertainties as shown in Table 5.

4 Responses to Items Identified in the 2016 Review

Our 2016 SoLID Run-Group proposal was deemed to be of high scientific merit, but there were a number of technical questions that were asked to be studied before final approval can be given. The following list is compiled from the TAC, Theory, and SoLID review reports, reordered according to topic. Our response to each item is also given.

4.1 SoLID Acceptance Simulations

The simulations for this measurement may benefit from tracking DEMP events through the full SoLID GEANT4 simulation (GEMC), particularly for kinematics with the lowest momentum protons (300 MeV/c).

This has been done. See Sec.

4.2 Experimental Background

The committee is convinced that the SIDIS background is likely not a major problem. However, an alternate approach (rather than SIDIS fragmentation functions) could be used. The primary background channel under study is $^3He(e,e'\pi^-)pp$ with the two undetected protons as spectators. The continuum background that can leak under the quasi-exclusive peak can be of the form $e+n \rightarrow e'+\pi^-+\Delta^+$ with the Δ^+ decaying to $p+\pi^0$.

The authors may want, however, to expand on possible contamination arising from Δ^{++} production on bound protons, and subsequent decay into π^+ and p.

We take this comment to mean the $e + p \rightarrow e' + \pi^- + \Delta^{++}$ background reaction, as otherwise there is no π^- in the final state to satisfy the offline event finder.

Neither $\pi^-\Delta$ final state is expected to be a substantial issue. We have investigated and compared the kinematics of the $\pi^- n$ and $\pi^-\Delta$ final states. The missing momentum of the $\pi^-\Delta$ state is about 500 MeV/c higher than the $\pi^- n$ final state, very similar to the difference between the DEMP and SIDIS distributions in Fig. 17. The 1 GeV/c missing momentum cut will eliminate about 50% of the $\pi^-\Delta$ events. In addition, the $\pi^-\Delta$ final state is centered about 300 MeV higher in missing mass than the $\pi^- n$ state, and will be further suppressed by a cut of approximately M_{miss} <1.05 GeV. We estimate the $\pi^-\Delta$ contamination remaining after the application of both cuts to be very similar to that already shown in Fig. 18.

4.3 Resolution and Energy Loss

The effects of Fermi-smearing, detector resolution, ionization energy loss and bremsstrahlung need to be clarified. Although they seem to all be included in Figs. 15 and 16, it was not clear which curves included which effects.

This has been clarified. See Sec.

4.4 Projected Uncertainties

The extraction of the term $|\sigma_{TT}^y + 2\epsilon\sigma_L^y|$ in Eqn. 8 from the other $\sin\beta$ and $\cos\beta$ terms requires good knowledge of the β-acceptance in each t-bin. This should be shown, in addition to the acceptance plots of Fig. 12.

This has been done. See Sec.

The collaboration should attempt to quantify the projected precision of the measured spin-dependent cross section. Although the asymmetry may have a smaller error bar, the spin-dependent cross section difference has a simpler interpretation. Measuring the spin-dependent cross section is also consistent with the opening sentence of Appendix A.

We agree that the extraction of these absolute cross sections would be very useful in terms of theoretical interpreation, but this is a very difficult question to answer at this early stage, given that SoLID is not designed for absolute cross section measurements. To be conservative, this proposal only relies on the extraction of the azimuthal asymmetry components from the target up-down polarization difference, where many systematic uncertainties cancel. This can be done reliably, even if the systematic uncertainties are otherwise too large for reliable absolute cross section measurements.

The quantitative estimate of detector efficiency and acceptance correction uncertainties, absolute kinematic offsets, etc. requires dramatically more study and a possible optimization of the SoLID detector system. After this proposal is accepted, we can continue our studies to see if this is a viable option for the SoLID Collaboration.

4.5 Fermi Momentum Effects

Fermi-momentum is not just a kinematic effect. It also affects the DEMP amplitude. The ^{3}He momentum distribution $\rho(p)$ is plotted in Fig. 10 (Appendix A). The weighted distribution $p^2\rho(p)$ peaks at $p_n \approx 60$ MeV/c. This means that the effective x_B is smeared by $\approx p_n/M \approx 6\%$. The significance of this effect should be discussed. Also, if the proton momentum resolution is good enough, it will be possible to correct for this effct, event-by-event.

We agree that if the proton momentum resolution is sufficiently good, it will be possible to correct for Fermi momentum on an event-by-event basis. We are familiar with this technique from our work with the A2 Collaboration at Mainz, for example. However, for the purposes of this proposal we take the less optimistic view that the proton resolution is likely not good enough.

The authors may want to switch off ^{3}He Fermi motion in their simulations and determine how large and in which kinematics they see a difference. Having evidence of non-negligible nuclear effects at an early stage would encourage theorists to extend now their calculations from inclusive to exclusive measurements for a timely and correct utilization of the data the authors propose to take. It would also be helpful to elaborate on the possible corrections in addition to Fermi motion, such as from binding and nucleon off-shell effects, as well as corrections beyond the impulse approximation from rescattering or final state interactions of the detected proton.

This has now been done, see Sec.

4.6 Dialog with Theorists

There are a number of important theory issues raised by this proposal. These probably cannot be fully resolved before re-submission, but it will be important to have a clear dialog with relevant theorists (and experimentalists) in place... Both Goloskokov and Kroll, and Liutti and Goldstein, have published estimates

of σ_T, based on transversity GPDs and a twist-3 helicity-flip pion distribution amplitude. One or the other of these theory groups should be engaged in a discussion of both the $|\sigma_L^y|$ and $|\sigma_{TT}^y|$ terms.

We have been in communication with Goloskokov and Kroll on the physics objectives of this proposal for some years, and they provided helpful comments to our 2016 proposal. With the additional time we had available for the 2017 proposal, Goloskokov and Kroll generously provided new asymmetry calculations, based on their best estimates of σ_T, σ_{TT} for SoLID kinematics. We are confident that approval of this proposal will raise the interest of other theorists to the physics potential of our measurements, and we will have dialog with them.

The QCD factorization theorem implies color transparency for the final state π^- in this proposal. Thus the $^3He(e,e'\pi^-)$ final state interactions (FSI) are identical with $^3He(e,e'p)$, just with a more exotic scattering amplitude. It is not practical to obtain full FSI calculations before resubmission, but a dialog should be started both with the groups doing FSI calculations, and the groups doing Deep Virtual calculations on light nuclei. Empirically, it will be useful to determine if the FSI 'peak' lies within the $^3He(e,e'\pi^-p)pp$ acceptance of this proposal.

As discussed in Sec. A.6 of the Appendix, we have made some estimates of FSI effects, based on an empirical parameterization of πN cross sections. Our estimates indicate that most FSI events are scattered outside the triple coincidence acceptance, and are effectively removed by our analysis cuts.

Elaborate, based on our findings.

Over the longer term, we will consult with theoretical groups for a more quantitative estimate of FSI effects. For example, Del Dotto, Kaptari, Pace, Salme and Scopetta recently published a study of FSI effects in SIDIS from a transversely polarized ^{3}He target [39] in SBS, SoLID and EIC kinematics. The SIDIS final state has more outgoing particles than DEMP, so there are more opportunities for FSI interactions there than the simple $\pi^- ppp$ final state considered here. Nontheless, they were able to show that the extracted Sivers and Collins asymmetries are basically independent of FSI, evaluated within the generalized eikonal approximation and a realistic distorted spin-dependent spectral function. A similar calculation for DEMP, after this proposal is approved, would be a natural extension of their work.

5 Summary

The transverse single-spin asymmetry in the exclusive $\vec{n}(e,e'\pi^-)p$ reaction has been noted as being especially sensitive to the spin-flip generalized parton distribution (GPD) $\tilde{E}$. Factorization studies have indicated that precocious scaling is likely to set in at moderate $Q^2 \sim 2-4$ GeV^2, as opposed to the absolute cross section, where scaling is not expected until $Q^2 > 10$ GeV^2. This relatively low value of Q^2 for the expected onset of precocious scaling is important, because it will be experimentally accessible at Jefferson Lab.

This measurement is complementary to a proposal to measure the longitudinal photon, transverse nucleon, single-spin asymmetry $A_L^\perp$ with the SHMS+HMS in Hall C [4]. The good resolution and reproducible systematic uncertainties of the SHMS+HMS setup allow the L–T separation needed to reliably measure this quantity. However, a wide $-t$ coverage is needed to obtain a good understanding of the asymmetry, and it always been intended to complement the SHMS+HMS $A_L^\perp$ measurement with an unseparated $A_{UT}^{sin(\phi-\phi_s)}$ measurement using a large solid angle detector. The high luminosity capabilities of SoLID make it well-

suited for this measurement. Since an L–T separation is not possible with SoLID, the observed asymmetry is expected to be diluted by the ratio of the longitudinal cross section to the unseparated cross section. This was also true for the pioneering HERMES measurements, which provided a valuable constraint to models for the $\tilde{E}$ GPD. The $A_{UT}^{\sin(\phi_S)}$ asymmetry can also be extracted from the same data, providing powerful additional GPD model constraints. This measurement is also important preparatory work for future measurements at the EIC, which will allow $A_{UT}^{sin(\phi-\phi_s)}$ to be directly compared for the $\vec{n}(e,e'\pi^-)p$ and $\vec{p}(e,e'\pi^+)n$ reactions over a broad kinematic range.

In our proposal, we will analyze the E12-10-006 event files off-line to look for $e-\pi^- -p$ triple coincidence events in SoLID for the case where the recoil proton is emitted $8^o < \theta < 24^o$. This study yields data that are a considerable advance over the HERMES measurement in terms of kinematic coverage and statistical precision.

A Monte Carlo model of Deep Exclusive π^- Production from the Neutron in ^{3}He

The Monte Carlo studies needed for this proposal require a reaction model for an experimentally unexplored region of kinematics, at higher values of Q^2, $-t$ and W than covered by existing data. This appendix describes the model and the constraints used.

A.1 Definition of the Cross Section and Single-Spin Asymmetries

The differential cross section for exclusive π production from the nucleon can be written as

$$\frac{d^5\sigma}{dE' d\Omega_{e'} d\Omega_\pi} = \Gamma_V \frac{d^2\sigma}{d\Omega_\pi}. \tag{21}$$

The virtual photon flux factor Γ_V is defined as

$$\Gamma_v = \frac{\alpha}{2\pi^2}\frac{E'}{E}\frac{K}{Q^2}\frac{1}{1-\epsilon}, \tag{22}$$

where α is the fine structure constant, K is the energy of real photon equal to the photon energy required to create a system with invariant mass equal to W and ϵ is the polarization of the virtual photon.

$$K = (W^2 - M_p^2)/(2M_p) \tag{23}$$

$$\epsilon = \left(1 + \frac{2|\mathbf{q}|^2}{Q^2}\tan^2\frac{\theta_e}{2}\right)^{-1}, \tag{24}$$

where θ_e is the scattering angle of scattered electron.

The two-fold differential cross section $\frac{d^2\sigma}{d\Omega_\pi}$ in the lab frame can be expressed in terms of the invariant cross section in centre of mass frame of the photon and nucleon,

$$\frac{d^2\sigma}{d\Omega_\pi} = J\frac{d^2\sigma}{dt d\phi}, \tag{25}$$

where J is the Jacobian of transformation of coordinates from lab Ω_π to t and ϕ (CM).

Following Ref. [16], we consider separately the unpolarized and polarized target contributions to the invariant photon nucleon cross section,

$$d\sigma = d\sigma_{UU} + d\sigma_{UT}. \tag{26}$$

In the one-photon exchange approximation, the unpolarized nucleon cross section for $n(e, e'\pi^-)p$ can be expressed in four terms. Two terms correspond to the polarization states of the virtual photon (L and T) and two states correspond to the interference of polarization states (LT and TT),

$$d\sigma_{UU} = \epsilon\frac{d\sigma_{\rm L}}{dt} + \frac{d\sigma_{\rm T}}{dt} + \sqrt{2\epsilon(\epsilon+1)}\frac{d\sigma_{\rm LT}}{dt}\cos\phi + \epsilon\frac{d\sigma_{\rm TT}}{dt}\cos 2\phi, \tag{27}$$

where ϕ is the angle between lepton plane and hadron plane (Fig. 3). The first two terms of Eqn. 27 correspond to the polarization states of the virtual photon (L and T) and last two terms correspond to the interference of polarization states (LT and TT). ϵ is the ratio of longitudinal to transverse virtual-photon fluxes

$$\epsilon = \left(1 + \frac{2|\mathbf{q}|^2}{Q^2}\tan^2\frac{\theta_e}{2}\right)^{-1}. \tag{28}$$

The constraints used to parameterize $d\sigma_{UU}$ are described in Sec. A.2.

The additional contribution when the target nucleon is transversely polarized can be parameterized [15,16] as

$$d\sigma_{UT} = -\frac{P_T}{\sqrt{1-\sin^2\theta\sin^2\phi_S}}\sum_{k=1}^{6}\sin\left(\mu\phi+\lambda\phi_S\right)\Sigma_k, \tag{29}$$

where ϕ_S is angle between the target polarization and lepton planes (Fig. 3), the Σ_k are given by

$$\Sigma_k = A_{UT}^{\sin\left(\mu\phi+\lambda\phi_S\right)_k} \times d\sigma_{UU}(\phi), \tag{30}$$

and the $\sin(\mu\phi+\lambda\phi_S)$ are the different azimuthal modulations. The calculation of $d\sigma_{UT}$ in the event generator is described in Sec. A.3.

A.2 Cross Section Model for Higher Q^2 Kinematics

A.2.1 Constraints

All of the following data were used as constraints on the parameterizations used in this model.

- From Hall C, precise L/T separated experimental data of exclusive electroproduction of π^- on ^{2}H are available up to $Q^2 = 2.57$ GeV^2, $-t = 0.350$ GeV^2 and $W = 2.168$ GeV [34].
- Also from Hall C, precise L/T separated experimental data of exclusive electroproduction of π^+ on ^{1}H are available up to $Q^2 = 2.703$ GeV^2, $-t = 0.365$ GeV^2 and $W = 2.127$ GeV [26], and separated σ_L and σ_T are measured up to $Q^2 = 4.703$ GeV^2 and $W = 2.2$ GeV [35] and [36].
- CLAS experiment E99-105 measured the unseparated exclusive π^+ cross section from ^{1}H at Q^2 up to 4.35 GeV^2 and $-t$ up to 4.5 GeV^2 [37].
- The HERMES collaboration measured the unseparated cross section for Q^2=3.44 GeV^2 and 5.4 GeV^2 [38] at W=4 GeV.

An additional constraint in our parameterization comes from the Vrancx-Ryckebusch (VR) model [40]. This is a Regge model with a parametrization of the deep inelastic scattering amplitude added to improve the description of σ_T. The description of σ_L in the model is constrained by a fit to the Hall C $p(e,e'\pi^+)n$ data from Ref. [**?**]. The model provides a good description of exclusive charged pion electroproduction above the resonance region. It has been checked for reliability against the Hall B and C data listed above, for $W > 2$ GeV, Q^2 from 0.35 to 4.98 GeV^2. The model is believed to be reliable for $-t \leq$0.5 GeV^2, but it overshoots the data for $-t >$0.5 GeV^2.

A.2.2 Parametrization of σ_L, σ_T, σ_{LT}, & σ_{TT}

For exclusive DEMP in SoLID, the kinematic region of interest for parametrization of $\sigma_{L,T,LT,TT}$ is Q^2 from 4.0 GeV to 7.5 GeV^2, $-t$ from 0 GeV^2 to 1.0 GeV^2, and we set $W = 3.0$ GeV. After the parametrization of $\sigma_{L,T,LT,TT}$ for $-t$ and Q^2, we used the same W dependence given by [**?**], which is $(W^2 - M^2)^{-2}$ where M is the proton mass. Our parametrization of all four cross sections is given in equations 31 to 34.

$$\sigma_L = \exp\left(P_1(Q^2) + |t| * P_1'(Q^2)\right) + \exp\left(P_2(Q^2) + |t| * P_2'(Q^2)\right) \tag{31}$$

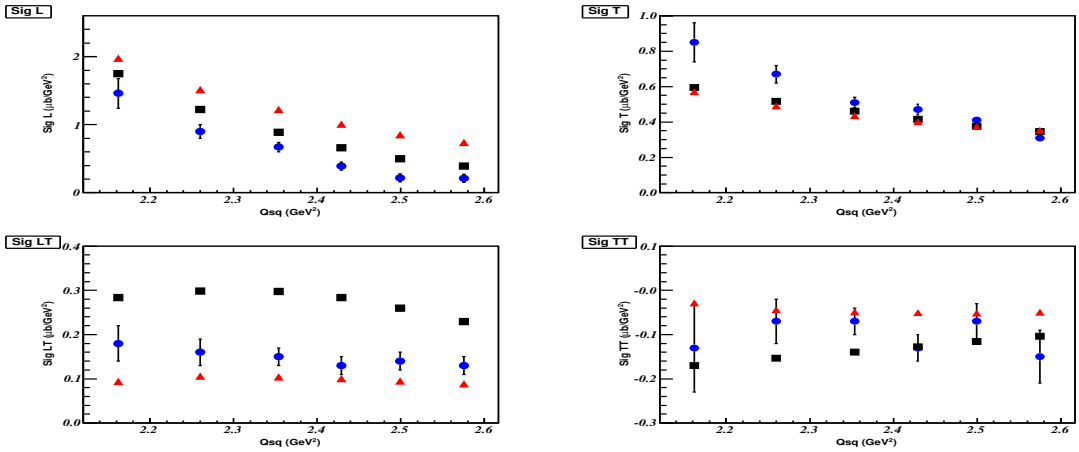

Figure 19: A comparison of last six points of table v of [34], the VR model, and our parametrization values vs. Q^2 for π^- electroproduction. Experimental data are shown in blue circles, VR model is shown in red triangles, and our parametrization is shown in black boxes. In each graph, the value of $-t$ is decreasing left to right from a maximum value 0.35 GeV^2 to 0.15 GeV^2. Value of W also decreases left to Right from 2.2978 GeV to 2.1688 GeV.

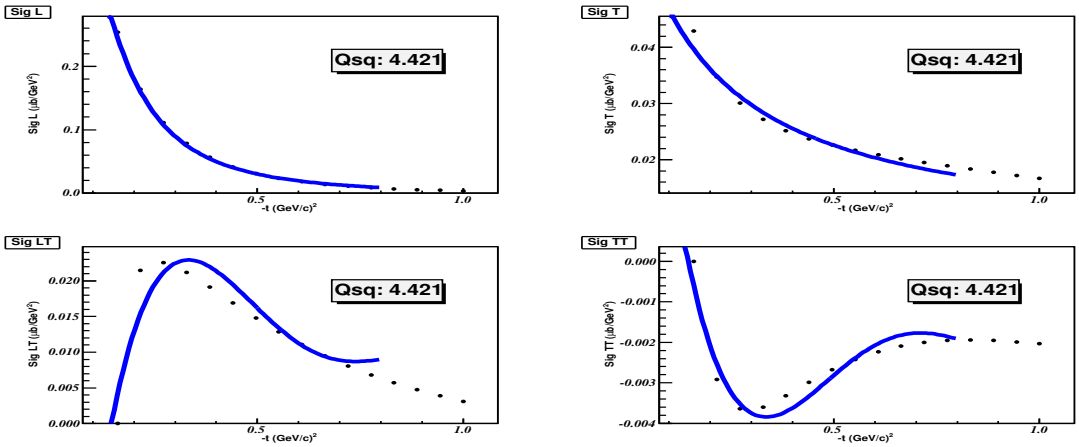

Figure 20: A comparison of parametrized $\sigma_{L,T,LT,TT}$ and VR model values at $Q^2 = 4.421$ GeV^2 and $W = 3.0$ GeV. Black points are VR model values and blue line is parametrized $\sigma_{L,T,LT,TT}$ given by equations 31 to 34.

$$\sigma_T = \frac{\exp\left(P_1(Q^2) + |t| * P_1'(Q^2)\right)}{P_1(|t|)} \tag{32}$$

$$\sigma_{LT} = P_5(t(Q^2)) \tag{33}$$

$$\sigma_{TT} = P_5(t(Q^2)) \tag{34}$$

Here, the parameters P_i are polynomial functions of i^{th} order. Each coefficient (P_i) of the fifth order

equations 33 and 34 is a further second order polynomial of Q^2. Deep exclusive π^- events are generated using a C++ code. The quality of parametrization is checked by plotting the parametrization functions of $\sigma_{L,T,LT,TT}$ versus the existing data and the VR model are shown in Figs. 19, 20.

There is no statement made that the cross section is calculated in the neutron rest frame from the 'vertex' kinematic quantities, and then transformed to the lab frame.

A.3 Parametrization of six Single-Spin Asymmetries

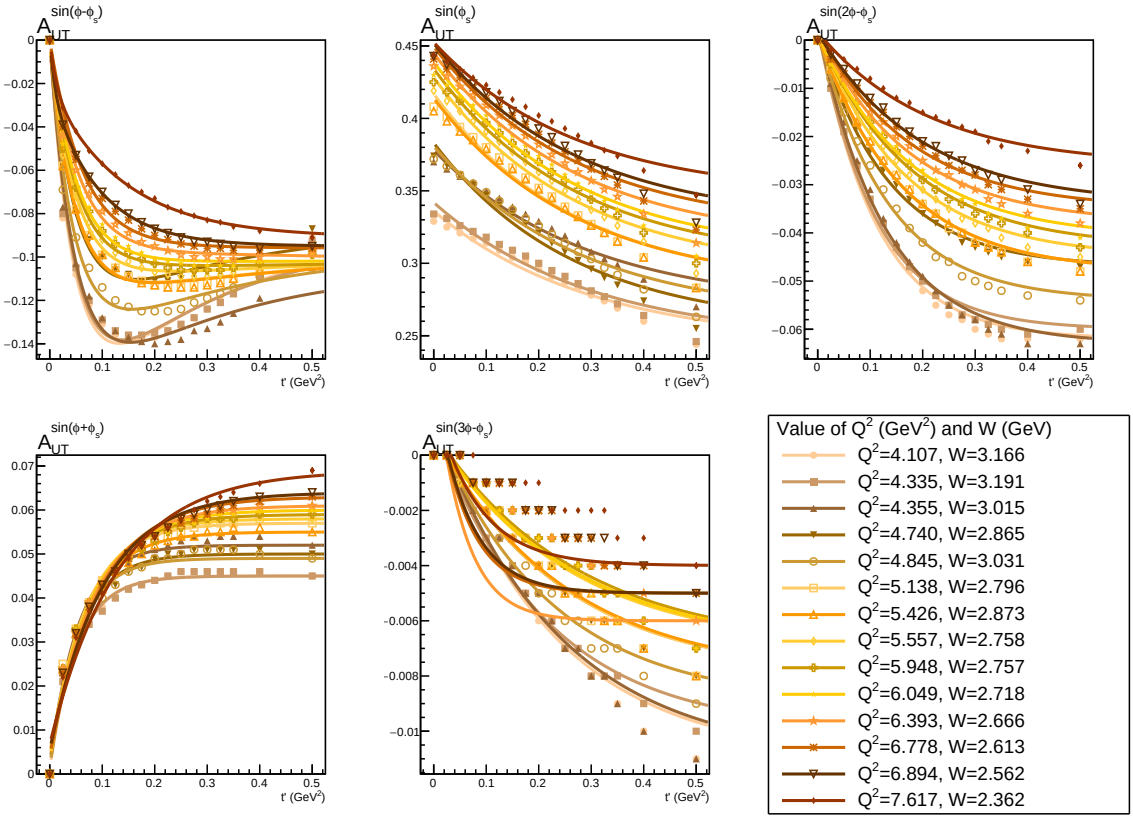

Figure 21: Parametrization of the five single spin asymmetries $A_{UT}^{\sin(\mu\phi+\lambda\phi_s)_k}$ vs. t' used in the event generator for this proposal. The points are the calculations by Goloskokov and Kroll [24] and the curves are our fit.

The single-spin asymmetries calculated for us by S.V Goloskokov and P. Kroll [24] have been used to approximate $d\sigma_{UT}$ in the DEMP event generator. Their $A_{UT}^{\sin(\mu\phi+\lambda\phi_s)_k}$ values are at discrete values of Q^2 from 4.107 to 7.167 GeV^2, W from 2.362 to 3.191 GeV, and t' from 0 GeV^2 to 0.5 GeV^2. There are six different azimuthal modulations defined as follows:

k	$\sin(\mu\phi + \lambda\phi_s)$
1	$\sin(\phi - \phi_s)$
2	$\sin(\phi + \phi_s)$
3	$\sin(\phi_s)$
4	$\sin(2\phi - \phi_s)$
5	$\sin(3\phi - \phi_s)$
6	$\sin(2\phi + \phi_s)$

These asymmetries are used to give

$$\Sigma_k = d\sigma_{UU}(\phi) A_{UT}^{\sin(\mu\phi+\lambda\phi_s)_k} \tag{35}$$

$$d\sigma_{UT} = -\frac{P_T}{\sqrt{1 - \sin^2\theta \sin^2\phi_s}} \sum_{k=1}^{6} \sin(\mu\phi + \lambda\phi_s)_k \Sigma_k \tag{36}$$

The $k = 6$ asymmetry ($(\mu, \lambda) = (2, 1)$) is not included in their calculation, and is taken to be zero, in accordance with the HERMES data [16]. The other five are calculated based on fits to their values. The following fits were used:

$$A_{UT}^{\sin(\mu\phi+\lambda\phi_s)_k} = \begin{cases} ae^{bx} - (a+c)e^{dx} + c, & k = 1 \\ ae^{bx} + c, & k = 2, 3, 4, 5 \end{cases} \tag{37}$$

where a, b, c, and d are fit parameters. The forms of these functions were chosen only to closely match the shape of the simulated data and are not based on any physical principle. These fits are done for each given value of Q^2 independently, as shown in Fig. 21. During event generation, the asymmetry is calculated from the fit for the two nearest values of Q^2. The asymmetry for the given event is then approximated by linear interpolation of the nearest values.

A.4 Target Neutron Fermi Momentum

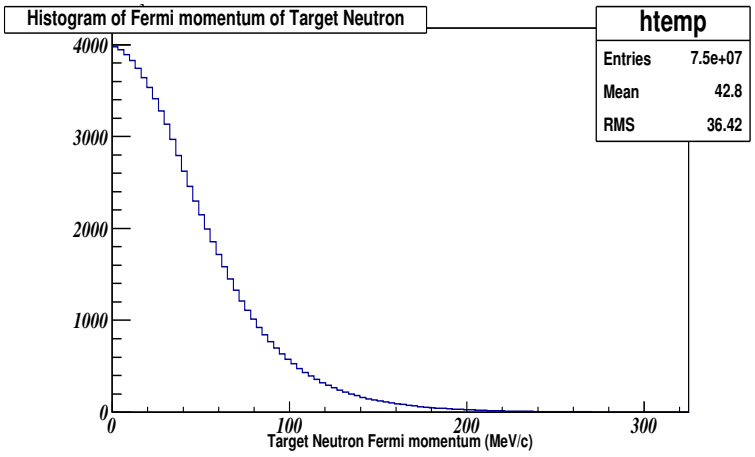

Figure 22: Fermi momentum spectral function of a target nucleon in ^{3}He generated according to the Argonne potential of Ref [41]. The horizontal axis is nucleon momentum in MeV/c.

A histogram of the spectral function of ^{3}He is shown in Fig. 22, generated according to Ref. [41]. Neutron momenta up to 300 MeV/c are generated according to this distribution, uniformly distributed in spherical coordinates. The quasi-free collision between the virtual photon and moving neutron is then transformed to the fixed neutron frame, after which the parameterizations of Secs. A.2.2, A.3 are applied. The outgoing particles are then transformed back to the lab frame for tracking.

A.5 Energy Loss and Multiple Scattering

There is energy loss for the incoming electron e, and the three outgoing particles: scattered electron e', π^- and recoil proton p by bremsstrahlung and ionization. The same code as given in SAMC (Hall A Single Arm Monte Carlo) [42] is used. This code is based on Sec. 33 (Passage of articles through matter) of the Review of Particle Physics by the Particle Data Group [43].

Incoming electron and three out going particles are deflected small angles by multiple scattering in the target, target window and in the air. This small deflection in the polar angle theta θ is calculated according to Subsection 33.3 (Multiple scattering through small angles) of the Review of Particle Physics by the Particle Data Group [43].

The incoming electron loses energy by bremsstrahlung and ionization, and suffers multiple scattering, in the target and in the target window. Both of these processes and the choice of neutron Fermi momentum are applied before the cross section terms σ_{uu} and σ_{UT} are calculated from the 'vertex' kinematic quantities.

The scattered electron, pion and proton lose energy by bremsstrahlung and ionization, and suffer multiple scattering, in the target, target window and in the air. The energy and momentum of these particles are corrected according to these processes prior to particle tracking.

A.6 Final State Interactions

A separate version of the model was made in which the outgoing π^- suffers πN final state interactions (FSI) with one of the recoil p in the residual nucleus.

The scattering of π^- by protons involves both the $T = 1/2$ and $T = 3/2$ isospin states. We model the $\pi^- p$ scattering via the empirical phase shift analysis of Rowe, Solomon and Landau [44]. In this case, the amplitude for the scattering of a spin-zero particle by a particle of spin-$\frac{1}{2}$ is described for each isospin channel by a set of partial wave amplitudes $f_\ell^{(+)}$, $f_\ell^{(-)}$ for the $j = \ell \pm \frac{1}{2}$ states. In terms of phase shifts, $f_\ell^{(+)}$ is

$$f_\ell^{(+)} \equiv \frac{1}{2ik}(e^{2i\delta_\ell^+} - 1) \tag{38}$$

with a similar expression for $f_\ell^{(-)}$. The phase shift δ_ℓ^+ will be complex if there is any inelasticity, which will occur for example for the reactions

$$\begin{aligned} \pi^- + p &\to \pi^+\pi^- p \\ &\to \pi^0\pi^0 n \\ &\to \pi^-\pi^0 p. \end{aligned} \tag{39}$$

The differential cross-section is written in terms of these phase shifts as

$$\frac{d\sigma}{d\Omega} = \left[\left|\frac{1}{k}\sum_\ell [(\ell+1)f_\ell^{(+)} + \ell f_\ell^{(-)}]P_\ell(\cos\theta)\right|^2 + \left|\frac{i}{k}\sum_\ell [f_\ell^{(+)} - f_\ell^{(-)}]\sin\theta \frac{dP_\ell(\cos\theta)}{d\cos\theta}\right|^2\right]. \tag{40}$$

πN phase shifts have been determined experimentally from near threshold up to several GeV. The dominant phase shifts for the $L_{2T,2J}$ states: S_{11}, S_{31}, P_{11}, P_{13}, P_{31}, P_{33} are very accurately known for centre of mass momenta up to 350 MeV/c. The phase shift parameterizations used in our model are dominated by the $\Delta(1232)$ and $N^*(1440)$ resonances. For further information, please see Ref. [45].

In our implementation of the FSI process, the Fermi momentum of one of the recoil protons was chosen according to Sec. A.4 and collided with the outgoing π^- in their mutual centre of mass frame. Outgoing π^- N were randomly generated, and the events weighted according to the differential cross setions of Eqn. 40. Events were generated for both the FSI and non-FSI versions of the model and the results compared, as described in the main text.

References

[1] Approved SoLID SIDIS experiment E12-10-006, "Target Single Spin Asymmetry in Semi-Inclusive Deep-Inelastic $(e, e'\pi^{\pm})$ Reaction on a Transversely Polarized ^{3}He Target at 11 GeV", $https://www.jlab.org/exp\_prog/proposals/14/E12-10-006A.pdf$

[2] SoLID Collaboration, "Solenoial Large Intensity Device Preliminary Conceptual Design Report", $http://hallaweb.jlab.org/12GeV/SoLID/files/solid\_precdr.pdf$

[3] A. Airapetian, Phys. Lett. **B 682** (2010) 345-350, arXiv:0907.2596 [hep-ex].

[4] PR12-12-005: D. Dutta, D. Gaskell, W. Hersman, G.M. Huber, et al., "The Longitudinal Photon, Transverse Nucleon, Single-Spin Asymmetry in Exclusive Pion Production".

[5] M. Diehl, Contribution to the eRHIC White Paper, arXiv:hep-ph/0010200.

[6] J.C. Collins, L. Frankfurt, M. Strikman, Phys. Rev. D **56** (1997) 2982.

[7] K. Goeke, M.V. Polyakov, M. Vanderhaeghen, Prog. Part. Nucl. Phys. **47** (2001) 401-515.

[8] A.V. Radyushkin, arXiv:hep-ph/0101225.

[9] A.W. Thomas, W. Weise, "The Structure of the Nucleon", J. Wiley-VCH, 2001.

[10] R.E. Marshak, Riazuddin, C.P. Ryan, "Theory of Weak Interactions in Particle Physics", J. Wiley, 1969.

[11] M. Penttinen, M.V. Polyakov, K. Goeke, Phys. Rev. C **62** (2000) 014024 1-11.

[12] A.V. Belitsky, D. Mueller, Phys. Lett. **B 513** (2001) 349-360.

[13] S. V. Goloskokov and P. Kroll, Eur. Phys. J. C **65**, 137 (2010), arXiv:0906.0460 [hep-ph].

[14] L.L. Frankfurt, P.V. Pobylitsa, M.V. Polyakov, M. Strikman, Phys. Rev. D **60** (1999) 014010 1-11.

[15] M. Diehl, S. Sapeta, Eur. Phys. J. C **41** (2005) 515, arXiv:hep-ph/0503023.

[16] Ivana Hristova, "Transverse-Target Single-Spin Azimuthal Asymmetry in Hard Exclusive Electroproduction of Single Pions at HERMES", Ph.D. thesis, Humboldt University of Berlin, December 13, 2007. $http://bib-pubdb1.desy.de/record/288884/files/desy-thesis-07-041.pdf?version=1$

[17] M. Vanderhaeghen, P.A.M. Guichon, M. Guidal, Phys. Rev. D **60** (1999) 094017 1-28.

[18] L.L. Frankfurt, M.V. Polyakov, M. Strikman, M. Vanderhaeghen, Phys. Rev. Lett. **84** (2000) 2589-2592.

[19] A.V. Belitsky, CIPANP 2003 proceedings. arXiv: hep-ph/0307256.

[20] L. Mankiewicz, G. Piller, A. Radyushkin, Eur. Phys. J. **C 10** (1999) 307-312.

[21] C.E. Carlson, J. Milana, Phys. Rev. Lett. **65** (1990) 1717.

[22] E12-06-101, "Measurement of the Charged Pion Form Factor to High Q^2", G.M. Huber, D. Gaskell, spokespersons.

[23] pCDR for the Science and Experimental Equipment for the 12 GeV Upgrade of CEBAF, June, 2004. V. Burkert et al., PAC18 Review of the Science Driving the 12 GeV Upgrade, July, 2000.

[24] S. V. Goloskokov and P. Kroll, private communications 2009-2017.

[25] S. V. Goloskokov and P. Kroll, Eur. Phys. J. A **47**, 112 (2011), arXiv:1106.4897 [hep-ph].

[26] H.P. Blok, et al., Phys. Rev. C **78** (2008) 045202.

[27] Approved SoLID SIDIS experiment E12-11-007, "Asymmetries in Semi-Inclusive Deep-Inelastic $(e, e'\pi^{\pm})$ Reactions on a Longitudinally Polarized ^{3}He Target at 8.8 and 11 GeV", *https* : *//www.jlab.org/exp*$_p$*rog/PACpage/PAC*37*/proposals/Proposals/New*%20*Proposals/PR* − 11 − 007*.pdf*

[28] Approved SoLID SIDIS experiment E12-11-108, "Target Single Spin Asymmetry in Semi-Inclusive Deep-Inelastic $(e, e'\pi^{\pm})$ Reactions on a Transversely Polarized Proton Target", *https* : *//www.jlab.org/exp_prog/proposals/*11*/PR*12 − 11 − 108*.pdf*

[29] Approved SoLID J/ψ experiment E12-12-006A, "Near Threshold Electroproduction of J/ψ at 11 GeV", *https* : *//www.jlab.org/exp*$_p$*rog/proposals/*12*/PR*12 − 12 − 006*.pdf*

[30] Approved SoLID SIDIS experiment E12-10-006A, "Dihadron Electroproduction in DIS with Transversely Polarized ^{3}He Target at 11 and 8.8 GeV", *https* : *//www.jlab.org/exp*$_p$*rog/proposals/*14*/E*12 − 10 − 006*A.pdf*

[31] Approved SoLID SIDIS experiment E12-11-108A, "Target Single Spin Asymmetry Measurements in the Inclusive Deep-Inelastic $\vec{N}(e, e')$ Reaction on Transversely Polarized Proton and Neutron (^{3}He) Targets using the SoLID Spectrometer" *https* : *//www.jlab.org/exp*$_p$*rog/proposals/*14*/E*12 − 11 − 108A_E12 − 10 − 006*A.pdf*

[32] Approved SoLID PVDIS experiment E12-10-007, "Precision Measurement of Parity-violation in Deep Inelastic Scattering Over a Broad Kinematic Range", *https* : *//www.jlab.org/exp_prog/PACpage/PAC*37*/proposals/Proposals/Previously*%20*Approved/E*12− 10 − 007*.pdf*

[33] J. L. Friar et al., Phys. Rev. C 42, (1990) 2310; C. Ciofi degli Atti, and S. Scopetta, Phys. Lett. **B404**, (1997) 223; R.W. Schulze and P.U. Sauer, Phys. Rev. **C56** (1997) 2293; F. Bissey, A.W. Thomas, and I.R. Afnan, Phys. Rev. **C64**, (2001) 024004.

[34] G. M. Huber *et al.*, Phys. Rev. **C91**, 015202 (2015).

[35] T. Horn *et al.*, Phys. Rev. Lett **97**, 192001 (2006).

[36] T. Horn *et al.*, Phys. Rev. **C78**, 058201 (2008).

[37] K. Park *et al.*, Eur. Phys. J. A **49**, 16 (2013). *http* : *//clas.sinp.msu.ru/cgi* − *bin/jlab/db.cgi?eid* = 36; *search* = *on*

[38] A. Airapetian *et al.*, Phys. Lett. B. **659**, (2008).

[39] A. Del Dotto, L.P. Kaptari, E. Pace, G. Salme, S. Scopetta, arXiv:1704.06182 [nucl-th].

[40] T. Vrancx and J. Ryckebusch., Phys. Rev. **C89**, 025203 (2014).

[41] R. Schivavilla and V. R. Pandharipande., Nucl. Phys. A. **449**, 219 (1986).

[42] Hall-A Single-Arm Monte Carlo Simulation Tool,
$https://userweb.jlab.org/\sim yez/Work/SAMC/$

[43] Particle Data Group, Chinese Physics C, **40**, 100001 (2016).

[44] G. Rowe, M. Solomon, R.H. Landau, Phys. Rev. C **18**, 584 (1978).

[45] T. Ericson, W. Weise, "Pions and Nuclei", Oxford University Press (1988).